Diplomarbeit

Post-mortem changes and autolysis in frontal lobe cells of *Sus scrofa*

a cellular and subcellular ultrastructural analysis via transmission electron microscopy

eingereicht von

Deniz Tafrali

zur Erlangung des akademischen Grades

Doktor(in) der gesamten Heilkunde

(Dr. med. univ.)

an der

Medizinischen Universität Graz

ausgeführt am

Lehrstuhl für Zellbiologie, Histologie und Embryologie

Gottfried Schatz Forschungszentrum

unter der Anleitung von

Assoz. Prof. Priv.-Doz. Mag. Dr.rer.nat., Leitinger, Gerd

Wien, den 30.10.2019

Eidesstattliche Erklärung

Ich erkläre ehrenwörtlich, dass ich die vorliegende Arbeit selbstständig und ohne fremde Hilfe verfasst habe, andere als die angegebenen Quellen nicht verwendet habe und die den benutzten Quellen wörtlich oder inhaltlich entnommenen Stellen als solche kenntlich gemacht habe.

Wien, am 30.10.2019 *Deniz Tafrali eh*

Preface and acknowledgements

As a young scientist, I am really honoured to start my research career with a research topic that is in my opinion the greatest subject of all: neuroscience. The incredible complexity, beauty and virtuosity of the orchestral interplay, called functional neuroanatomy, is, in my view, the holy grail of science. With this humble admiration for the subject, I finished my work in a meticulous way and with perfection bordering on insanity. It was neither easy nor very convenient to constantly critically question your own knowledge, ability and general attitude about complex scientific topics. But: it was worth all the trouble.
This work was written in a time period over two years and in three continents. Hereby I would like to pay tribute to all the wonderful cities in which I wrote parts of my diploma thesis by now mentioning them: Graz, Prague, Ellwangen, Salzburg, Stockholm, London, Cambridge, New York, Denver, Bibione, Lignano, Crikvenica, Barcelona, Athens, Istanbul, Cinarcik, Bellagio, Menaggio, Cologne, Munich, Hamburg, Stuttgart, Berlin, Reykjavík, Amsterdam and of course Vienna.
Without further ado: I hope you learn a lot while reading this diploma thesis and wish that you enjoy studying it. And as always, do not forget to “sapere aude!”

At this point I would like to thank my little sister Cansu Tafrali for her support and her outstanding, keen scientific eye, which had a decisive influence on the scientific correctness of my diploma thesis. Further, I would like to thank my old friend and brother, Sinan Barus, for every evening we chatted about ancient and modern philosophy, science theory, or highly complex scientific concepts. Whether in our early years in McDonalds restaurants or later in various hookah bars - these evenings were life lessons for me and made me the scientist and human I am today.
Also, I would like to thank my dear professor Gerd Leitinger for the opportunity to write such an interesting scientific work. In addition, I am very grateful for the many important and elementary notes, instructions and lessons that I could enjoy with him and without which I could never have written this work.
Furthermore, I would like to thank Mariella Sele and Stefan Wernitznig for their formidable scientific input as well as their help. This work is embedded in a project involving the University Clinic for Neurology of the LKH Graz, the Institute of Pathology of the Medical University of Graz and the Analytical Chemistry Department of the Karl-Franzens University of Graz (Funded by the Austrian Science Foundation FWF, project P 29370).

Zusammenfassung

Einführung

Es gibt eine geringe Anzahl an Studien über post-mortale Veränderungen und Autolyse in Säugetier-Frontallappenzellen. Diese Arbeit trägt daher zum grundlegenden Verständnis des postmortalen neuronalen (und glialen) Zelltods durch Autolyse bei.

Material und Methoden

Als Versuchstier haben wir ein Exemplar des eurasischen Hausschweins verwendet. Nachdem das Schwein getötet worden ist, bereiteten wir in einem Post-Mortem-Intervall (PMI) von 0, 3, 6 und 12 Stunden Gewebeproben seines Frontallappens vor. Zu jedem Zeitpunkt haben wir das Gewebe mit einer Mischung aus Glutaraldehyd und Formaldehyd fixiert. Danach wurde es erneut mit Osmiumtetroxid fixiert, um schließlich in TAAB-Einbettungsharz eingebettet zu werden. Anschließend wurde die Probe dünn geschnitten und mit Platinblau und Bleicitrat kontrastiert. Zur Analyse der Proben verwendeten wir die Transmissionselektronenmikroskopie.

Ziele

Unser Ziel war es, Kriterien für die Post-Mortem-Autolyse zu definieren und anhand dieser Kriterien zu untersuchen, inwieweit eine Post-Mortem-Autolyse in Frontallappenzellen des eurasischen Hausschweins auftritt.

Ergebnisse

Es wurden die ultrastrukturellen Veränderungen von 51 Frontallappenneuronen, -astrozyten und -oligodendrozyten untersucht. Nach 12 h nahm der Durchmesser der neuronalen Zellen tendenziell ab (Neuronen: 12,61 µm bis 11,25 µm; Pyramidenzellen: 23,15 µm bis 14,24 µm), während der Durchmesser der Gliazellen eher zunahm (Astrozyten: 8,9 µm bis 12,4 µm; Oligodendrozyten: 9,73 µm bis 10,41 µm). In allen Frontallappenzellen trat ab 3 h eine Chromatinkondensation auf. Eine vollständige Ablösung der Ribosomen vom rER wurde in fast keiner der untersuchten Zellen gefunden (insgesamt 1:51). Die Vakuolisierung des Zytoplasmas wurde zum ersten Mal nach 3 Stunden beobachtet. Das Auftreten von Lysosomen war in allen PMIs und allen Zellen hoch (84,6% nach 0 h bis 100% nach 12 h).

Diskussion

Diese deskriptive Arbeit bestätigt mehrere autolytische ultrastrukturelle Veränderungen in Nerven- und Gliazellen, die bereits bei anderen Versuchstieren beschrieben worden sind. Die Chromatinkondensation, das Schrumpfen von Neuronen, das Anschwellen von Gliazellen, die intrazytoplasmatische Vakuolisierung und das Auftreten von Lysosomen sind Hinweise auf postmortale Autolyse. Das Auftreten von rER ohne Ribosomen und der strukturelle Zerfall aller Mitochondrien sind vergleichsweise unzuverlässige Marker für die postmortale Autolyse.

Abstract

Introduction

Publications on post-mortem changes and autolysis in mammalian frontal lobe cells are scarce, especially when it comes to its early mechanisms. This thesis therefore contributes to the fundamental understanding of post mortal neuronal (and glial) cell death through autolysis.

Material and methods

We used one specimen of the eurasian domestic pig as our study animal. After the pig was killed, we prepared tissue samples from its frontal lobe in a post-mortem interval (PMI) of 0, 3, 6 and 12 h. At every point in time, we fixed the tissue with a mixture of glutaraldehyde and formaldehyde. Afterwards it was fixed again with osmium tetroxide to finally be embedded in TAAB embedding resin. Subsequently the sample was thin sectioned and contrasted with platinum blue and lead citrate. To analyse the samples, we used transmission electron microscopy.

Aims

The aim was to carry out the criteria for post-mortem autolysis as well as to use these criteria to investigate to which degree post-mortem autolysis in frontal lobe cells of the Eurasian domestic pig occurs.

Results

Ultrastructural alterations of 51 frontal lobe neurons, astrocytes and oligodendrocytes were investigated. After 12 h the diameter of neuronal cells tended to decrease (neurons: 12,61 µm to 11,25 µm; pyramid cells: 23,15 µm to 14,24 µm) while glial cells rather gained in diameter (astrocytes: 8,9 µm to 12,4 µm; oligodendrocytes: 9,73 µm to 10,41 µm). Chromatin condensation occurred in all frontal lobe cells beginning at 3 h. Complete ribosome detachment from the rER was not found in nearly any investigated cell (1:51 overall). Vacuolization of the cytoplasm was first seen at 3 h. The occurrence of lysosomes was high throughout the PMIs in all cells (84.6 % at 0 h to 100 % at 12 h).

Discussion

This descriptive work confirms several autolytic ultrastructural changes in neural and glial cells described in other study animals. Chromatin condensation, neurons shrinking, glial cells swelling, intracytoplasmic vacuolization and the occurrence of lysosomes are valid

indicators for autolysis. The occurrence of rER without any ribosomes and structural disintegration of all mitochondria are comparatively unreliable markers for autolysis.

Inhaltsverzeichnis

Glossar und Abkürzungen

- ATP = adenosine triphosphate
- CBI = catastrophic brain injury
- FGM = frontal grey matter
- FWM = frontal white matter
- h = hours
- LMP = lysosome membrane permeabilization
- M = molar mass
- min = minutes
- µm = micrometre
- n = number
- nm = nanometre
- PMI = post-mortem interval
- rER = rough endoplasmic reticulum
- TEM = transmission electron microscopy
- vs. = versus

Abbildungsverzeichnis

Tabellenverzeichnis

1 Introduction

During the death of a person, major changes to the cells of the human brain occur very quickly. Since there are not enough studies on post-mortem changes in the human brain within the first 12 hours of death, we do not know what kind of cellular and subcellular post-mortem alterations occur in the human brain and how they evolve over time. To investigate such post-mortem changes, one must remove brain tissue from the subject's skull in a very short time after death. Because of moral, ethical, and legal limitations, acquiring human brain tissue immediately after the determination of death is not possible. To be able to pursue this question, we therefore needed a study animal whose brain tissue we can remove immediately after death.

Because the porcine brain is more similar to the human brain than the brain of small animals like rats or mice and due to its commercial availability (Lind et al., 2007, pp. 729–732), we used one specimen of the domestic house pig (*Sus scrofa*) as our study animal. Also, because parts of the porcine frontal lobe are especially vulnerable to hypoxic insults (Stinnett et al., 2017, p. 22), we decided to investigate the frontal white and grey matter of our pig. Moreover, we concentrated on ultrastructural alterations regarding autolysis in a post-mortem interval (PMI) of 0 h, 3 h, 6 h and 12 h.

Before we begin to describe the post-mortem changes and autolysis, we must first define, what death is. Death is defined as "the permanent loss of capacity for consciousness and loss of all brainstem functions […] [which] may result from [the] permanent cessation of circulation and/or after catastrophic brain injury" (Tomlinson, 2012, p. 38). Furthermore, there is no exact point in time where an organism is dead - death is a process. Therefore, one can categorize and describe the happenings underlying the process of death as followed.

If a mammalian animal undergoes a catastrophic brain injury (CBI), such as but not limited to traumatic brain injury, cerebrovascular accidents or hypoxic-ischemic encephalopathy (Tomlinson, 2012, p. 17), normally the process of dying begins. Shortly after a CBI, there is lack of oxygen in the brain cells due to the cessation of blood-circulation. That leads to an ATP depletion, followed by failure of the sodium pump (Fricker et al., 2018, p. 820). This results in a biochemical switch to an anaerobic metabolism and an absence of the citric acid cycle (Donaldson and Lamont, 2013, p. 7). As a result of this processes, the following occurs: the cell body swells and the plasma membrane depolarizes, which consecutively opens voltage gated sodium and calcium channels (Fricker et al., 2018, p. 820). Because calcium pumps also use ATP as their preferred energy source, they start to

fail as well (Fricker et al., 2018, p. 820). The consequence is an elevation of intracytoplasmic calcium that leads to an activation of proteases, phospholipases and mitochondrial permeability transition (Fricker et al., 2018, p. 820). No later than now, manifold regulated and accidental cell death mechanisms can occur, depending on the circumstances (Fricker et al., 2018; Galluzzi et al., 2018).

Now that we know how death is defined and which immediate pathophysiological changes the brain of the organism is subject to while it deceases, we can start to investigate the concept of post-mortem changes.

Investigating any process of a single cell in a mammalian or rodent organism is always confounded if one disregards possible environmental and cell-bound-factors. In this case such cell-bound factors are influencing our investigated cells (frontal lobe cells) dramatically. Both for the sake of completeness and for a better understanding of the concept of autolysis, we now elucidate the most common post-mortem changes known as well as the factors influencing said changes.

Pallor mortis describes the post-mortem paleness of blood-devoid areas of the skin (Schäfer, 2000, p. 81). The term algor mortis is used to describe the equilibration of the temperature of a dead body with the temperature in the environment (Tsokos and Byard, 2016, p. 18). The bluish-violaceous to purple discoloration of blood-filled body parts after 30 to 180 min is called livor mortis (Tsokos and Byard, 2016, p. 10). The post-mortem change rigor mortis refers to the muscular stiffness that occurs in a dead body due to ATP depletion in the contractile actomyosin compound of muscles (Tsokos and Byard, 2016, pp. 15–16). Autolysis is a key post-mortem change, defined as the ‘self-digestion’ of tissue following the breakdown of a cell through endogenous substances (Tsokos and Byard, 2016, p. 19). Decomposition or putrefaction is the bacterial degradation of organs and soft tissues (Tsokos and Byard, 2016, p. 20).

The velocity of the occurrence of all post-mortem changes (including autolysis) is influenced by certain intrinsic and extrinsic factors. The physical status of the organism at the time of death is an important factor for the acceleration or deceleration of post-mortem changes (Dettmeyer, 2011, p. 401). The age, physical constitution, pre-existing diseases, such as fever, sepsis, or injuries, also have a tremendous influence on post-mortem alterations of the body (Dettmeyer, 2011, p. 401). Furthermore, the storage and therefore the type and duration of the position of the body influences post-mortem changes (Dettmeyer, 2011, p. 401). Finally, the weather conditions have a great effect on the speed

of post-mortem changes (Dettmeyer, 2011, p. 401). Especially the temperature, but also the humidity of the environment are important factors (Dettmeyer, 2011, p. 401; Tsokos and Byard, 2016, p. 10).

Because we are especially interested in autolysis regarding the frontal lobe of our study animal, we will now further elucidate the definition of the term and the underlying ultrastructural changes known to the literature.
The Nomenclature Committee on Cell Death does not mention the term *autolysis* in their 2018 review paper about the molecular mechanisms of cell death (Galluzzi et al., 2018). Instead of autolysis, they define the terms *autosis*, *autophagy-dependent cell death* and *lysosome-dependent cell death* (Galluzzi et al., 2018, p. 489).
Other authors do define autolysis, but with different levels of accuracy. Tsokos and Byard describe autolysis as the 'self-digestion' of tissue following the breakdown of a cell through endogenous substances (Tsokos and Byard, 2016, p. 19). Fricker et al. coin the term *lysosomal cell death* as a synonym for autolysis and define it as "cell death resulting from lysosomal membrane permeabilization (LMP)", by which lysosomes get 'leaky' due to different intrinsic or extrinsic biochemical factors that furthermore lead to the digestion of the cell through lysosomal enzymes (Fricker et al., 2018, p. 825).
The problem with a uniformed definition of autolysis lies in the intend of the usage of the term. We can refer to autolytic processes in a single cell of a living organism which are triggered due to LMP (Fricker et al., 2018, p. 825), or we can refer to autolysis as the aseptic breakdown of tissues and cells due to the endogenous release of proteases in a dying organism (Harle, 2019). Due to our study design (and therefore intend) we chose the latter definition. To differentiate these two definitions of the same term, we name the autolytic processes in a dying organism *post-mortem autolysis* rather than solely autolysis, which we use for a single cell-cell death mechanism in living organisms.
Regarding previous ultrastructural studies investigating the post-mortem changes and autolysis of brain cells (neurons, astrocytes and oligodendrocytes) there are a few authors to mention.
Suzuki describes post-mortem astrocyte swelling, occurrence of microvacuoles in neurons that underwent focal ischaemia, intracytoplasmic vacuoles in astrocytes that formed after global ischaemia, an increase of free ribosomes in the cytoplasm due to the detachment of ribosomes from the ER after 1 h and mitochondrial swelling in neurons after 1 h in rats (Suzuki, 2013, pp. 25; 46–49).

Sheleg et al. showed an occurrence of lysosomes as early as 6 h post-mortem with a slightly swollen appearance as well as mitochondrial swelling in neurons after 3 h (Sheleg et al., 2008, pp. 292–293).
Kalimo et al. describe chromatin clumping occurring as soon as 10 min post-mortem, ribosome detachment from the rER after 30 min post-mortem as well as rounded mitochondria with a less dense matrix, a slight swelling with occasional floccular densities inside the matrix and post-mortem astrocyte swelling in cat brains (Kalimo et al., 1977, p. 209).
According to Dettmeyer et al., chromatin agglutination in nerve cells takes place as soon as a few minutes after ischemic or hypoxic brain damage (Dettmeyer, 2011, p. 420).
Xu et al. describe chromatin clumping at 6 h post-mortem, shrinking of neurons of mice after 24 h in ischemic-hypoxic brain injury, intense vacuolization of mouse neurons paired with the appearance of numerous autophagosomes after 24 h in ischaemia, a rise in the count of lysosomes from 3 h to 12 h and fragmented ER after 6 h post-mortem in neurons with regards to autolysis (Xu and Zhang, 2011, p. 1092).
Garcia et al. state that chromatin clumping is seen at 6 h post-mortem, while neurons shrink, and oligodendrocytes and astrocytes tend to swell (Garcia et al., 1978, pp. 86–88). Also, the occurrence of many big vacuoles in neurons after regional brain ischaemia and swelling in astrocyte mitochondria as well as the appearance of matrical densities after 7 h post-mortem is observable (Garcia et al., 1978, pp. 86–88).
Panickar et al. describe ischemic astrocyte swelling and an increase of the count of ER in astrocytes after ischaemia as well as an overall rise in the count of mitochondria in astrocytes (Panickar and Norenberg, 2005, pp. 289–290).

To either support or challenge these findings this work conducted a cellular and subcellular ultrastructural study via transmission electron microscopy to investigate cellular and subcellular post-mortem changes and autolysis in frontal lobe cells of *Sus scrofa*. Furthermore, the aim of this work was to carry out the criteria for post-mortem autolysis as well as to use these criteria to investigate if and to which degree post-mortem autolysis in frontal lobe cells of in the Eurasian domestic pig (*Sus scrofa domesticus*) occurs.

2 Material and methods

We used one specimen of the Eurasian domestic pig (*Sus scrofa domesticus*) as our study animal. Prior to this thesis, the specimen preparation had been performed by Mariella Sele. Sectioning was done by Mariella Sele, Elisabeth Bock, and Elisabeth Pritz.

2.1 Tissue preparation

After the pig was killed, we prepared tissue samples from its frontal lobe at predefined specific moments in time (0 h, 3 h, 6 h and 12 h post-mortem). We examined 2 samples for every time point, both from grey and white matter areas in the frontal lobe 16 samples in total. The samples were fixed with a mixture of 2 % glutaraldehyde and 2 % formaldehyde in 0.1 M sodium cacodylate buffer, pH 7.4. After rinsing in the same buffer, the tissue was post fixed in 2 % osmium tetroxide solution and embedded in TAAB® embedding resin.

2.2 Electron microscopy

Subsequently each sample was sectioned at a thickness of 70 nm using either a Leica® UC6 or UC 7 ultramicrotome and contrasted with platinum blue and lead citrate solutions. The scope of this diploma thesis was to analyse the samples using a *Zeiss EM900®* Transmission Electron Microscope.

2.3 Autolytic criteria

For evaluating the post-mortem autolytic changes, we summarized selected ultrastructural criteria from the literature and categorized these into (a) whole cell ultrastructural changes including the nucleus and (b) subcellular ultrastructural changes (Tab. 1).

Tab. 1 Criteria for the autolysis of frontal lobe cells of Sus scrofa. The systematic structure of the table is hierarchically structured from the left to the right: First the criteria is classified in either a cellular or subcellular category. Then a title is given to every criterion. Finally, there is a description of the criteria which also contains the way each criterion is applied to the images. On the right hand side, we listed the references supporting our autolytic criteria.

Category	Criteria title	Description	References
Cellular changes	Cell diameter	Maximum diameter of cell bodies in an image with a cross-section of a nucleus with disregard of dendrites and axons given in µm	[1]
	Condensed chromatin	Existence of dense heterochromatin areas inside the nucleus with disregard of the location (Example: Fig. 4). Evaluation only within the borders of the cell. Binary decision: 0 = means fully euchromatic nucleus; 1 = at least one locus of condensed heterochromatic chromatin in nucleus	[2]

	Intracytoplasmic vacuolization	Single-membraned multiple small vacuoles in the cytosol or cell organelles. Evaluation of the complete image. Binary decision: 0 = there are no vacuoles visible; 1 = multiple small cytoplasmatic inclusions that are either apparent inside the cytosol and significantly smaller than most of the smooth or rough endoplasmic reticula inside the same cell or appear inside of cell organelles where there are normally are no such vacuoles.	[3]
Subcellular changes	Unphysiological ER	Unphysiological appearance of the ER. Evaluation only within the borders of the cell. Binary decision: 0 = smooth and rough ER apparent, either with or without swelling of cisternae (either normal, elongated or circular, swollen ER); 1 = all of the ER hast to be (a) circular and not elongated in its structure and (b) there should not be any rough ER with attached ribosomes, especially not near the nucleus, as a sign of the detachment of ribosomes from the ER	[4]
	Mitochondrial structure	Unphysiological appearance of mitochondria. Evaluation of the complete image. Binary decision: 0 = at least one mitochondrion with normal appearance of its cristae and continuous membranes; 1 = not a single mitochondrion with normal appearance of its cristae and continuous membranes	[5]
	Autolytic apparatus	Occurrence of lysosomes, autophagosomes and/or autolysosomes (diagnosis via (Kuehnel and Kuehnel, 2003, p. 34; Pavelka and Roth, 2015, pp. 148–149). Evaluation only within the borders of the cell. Binary decision: 0 = no lysosome/ autophagosome/ autolysosome visible inside the borders of the cell; 1 = at least one lysosome/ autophagosome/ autolysosome found inside the borders of the cell	[6]

[1]Swelling of astrocytes and parts of astrocytes (Suzuki, 2013, p. 46) (Garcia et al., 1978, p. 88; Kalimo et al., 1977, p. 214; Panickar and Norenberg, 2005, p. 289; Suzuki, 2013, p. 46); Shrinkage of neurons (Garcia et al., 1978, p. 88); Swelling of Oligodendrocytes (Garcia et al., 1978, p. 88). [2] Chromatin clumping in (Dettmeyer, 2011, p. 420; Garcia et al., 1978, p. 88; Kalimo et al., 1977, p. 207; Sheleg et al., 2008, p. 293; Xu and Zhang, 2011, p. 1092). [3]Intracytoplasmic vacuolization (Garcia et al., 1978, p. 88; Suzuki, 2013, p. 48; Xu and Zhang, 2011, p. 1092). [4]Detachement of ribosomes, disappearance of ribosomes, swelling of ER (Kalimo et al., 1977, p. 209; Sheleg et al., 2008, p. 292; Suzuki, 2013, p. 47; Xu and Zhang, 2011, p. 1090). [5]Swollen mitochondria and disintegrated cristae (Kalimo et al., 1977, p. 209; Sheleg et al., 2008, p. 295; Suzuki, 2013, p. 51; Xu and Zhang, 2011, p. 1092). [6]Appearance of autolytic organelles (Martínez et al., 2019; Xu and Zhang, 2011, p. 1092).

2.4 Database

Before we took the images, we created and structured a systematic directory folder as an image database. For a better understanding of the database structure, we used the hours of

the PMI and the areas of the brain, where the samples were taken from, as the folder names for each of the five samples of every hour and white or grey matter area (Fig. 1).

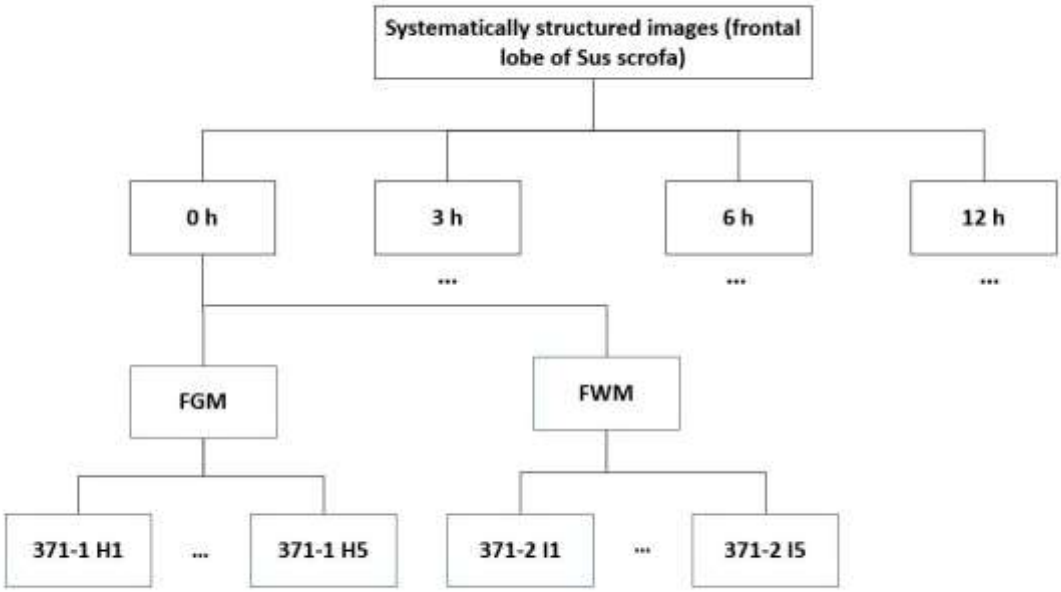

Fig. 1 Directory structure of the systematically structured images from the frontal lobe of our specimen of Sus scrofa. We created four subfolders under one main folder at the top of the diagram (systematically structured images (frontal lobe of Sus scrofa). These four folders represent the hours of the PMI. Each of these folders have their own subfolders each containing images from the five frontal grey matter (FGM) and frontal white matter (FWM) grids, which are again labelled with specific strings (e. g. 371-1 H1).

2.5 Camera, graphic viewers, magnification and strategy of photography

The images were taken with a Tröndle® camera (2k side mounted wide-angle camera, model 7899; software: Tröndle Image SP version 1.2.8). We took 147 images overall (Tab.) and investigated them with two graphic viewer programs on a computer with a Windows® operating system: ImageJ® (64-bit version with Java 1.8.0) for the measurement of the maximum cell diameter and IrfanView 4.53® for the investigation of the remaining autolytic criteria.

Tab. 2 Number of images taken overall, per brain matter and PMI. For name of folder see 2.4

Images taken	Name of folder	Brain matter	PMI
10	371-2 J1	FGM	0 h
2	371-2 J2		
19	371-1 H1	FWM	
8	371-1 H2		
21	371-4 L1	FGM	3 h
17	371-3 K1	FWM	
23	371-6 N1	FGM	6 h
17	371-5 M1	FWM	
9	371-8 P1	FGM	12 h

17	371-7 S1	FWM
4	371-7 S2	
147	*images overall*	

Furthermore, we used a standard magnification of 3000x when taking a photograph of a cell body. We photographed cell bodies if we (a) found a nucleus and (b) there were no or only a negligible number of contrasting artefacts. If we found a nucleus, we took a second image at a higher magnification or 12000x of areas inside the cell boundaries relevant to our autolytic criteria. Such areas were especially the nucleus, endoplasmic reticula near the nucleus, any form of double-membraned structures inside the cell boundaries as a hint for autophagosomes or -lysosomes (Pavelka and Roth, 2015, pp. 148–149) as well as mitochondria, round dark structures in a size from 100 nm to 1200 nm as a hint for lysosomes (Kuehnel and Kuehnel, 2003, p. 34) and multiple small single-membraned vacuoles. Additionally, we also examined areas outside of these boundaries regarding the occurrence of multiple small single-membraned vacuoles as well as mitochondria.

2.6 Statistical analysis

After taking all pictures, we investigated every image for our autolytic criteria and inserted the results in a Excel table for our data collection. An excerpt of this data table is seen in Tab. 3.

Tab. 3 Data table about the autolytic criteria maximum cell diameter, condensed chromatin, vacuoles and unphysiological ER at 3 hours post-mortem. We categorized each cell body with a brain region (FWM or FGM), cell group (neuron or non-neuron) and a cell type (neuron, pyramid cell, astrocyte or oligodendrocyte). The numbers 0 and 1 stand for either yes, the autolytic criterion is found in the cell (= 1) and no, the autolytic criterion is not found in this cell (=0). The last row shows the percentage of the overall occurrence of each criterion listed.

hour in PMI	brain region	cell group	cell type	cell diameter	condensed chromatin	vacuoles	ER
3	FGM	Non-Neurons	Astrocyte	11,1	1	0	0
3	FGM	Non-Neurons	Astrocyte	13,4	1	0	0
3	FGM	Non-Neurons	Astrocyte	15,29	1	1	0
3	FGM	Non-Neurons	Astrocyte	14,82	1	1	0
3	FWM	Non-Neurons	Astrocyte	16,7	1	0	0
3	FWM	Non-Neurons	Astrocyte	9,2	1	0	0
3	FGM	Neurons	Neuron	9	1	0	1
3	FWM	Non-Neurons	Oligodendrocyte	7,1	1	1	0
3	FWM	Non-Neurons	Oligodendrocyte	9,53	1	0	0
3	FWM	Non-Neurons	Oligodendrocyte	10,7	1	0	0
3	FWM	Non-Neurons	Oligodendrocyte	12,94	1	0	0
3	FWM	Non-Neurons	Oligodendrocyte	11,73	1	1	0
3	FGM	Neurons	Pyramid cell	13,56	1	1	0
3	FGM	Neurons	Pyramid cell	15,91	1	1	0
					100,00%	**42,86%**	**7,14%**

FGM = frontal grey matter, FWM = frontal white matter

Regarding the statistical analysis of the maximum cell diameter in µm we used the arithmetic mean, calculated by adding all measured diameters for each cell body of a single type at each time point and then dividing by the number of cells.
For the remaining autolytic criteria, we also used the arithmetic mean. We worked with dimensionless values in form of binary 0 or 1 decisions and added every single binary decision for every hour together. After that we divided the result by the number of cells (=arithmetic mean). As a result, we received the percentage of the occurrence of the autolytic criteria (Tab. 4).

2.7 Ultrastructural differentiation of neurons, pyramid cells, astrocytes and oligodendrocytes

To differentiate between neurons, astrocytes and oligodendrocytes, we first investigated grey and white matter separately. While working with white matter, we could exclude the possibility of finding any neuronal cell bodies, which enabled us to learn how to recognise cell bodies of glial cells. To furthermore distinguish fibrous astrocytes from oligodendrocytes (protoplasmic astrocytes are mainly found in grey matter (Matyash and Kettenmann, 2010, p. 3)), we adhered to ultrastructural differences between both type of cells described in the literature.
Astrocytes for example show a less dense cytoplasm than oligodendrocytes (Pannese, 2014, p. 199), may have glycogen particles in the size of 20 – 40 nm (Pannese, 2014, p. 201), have lighter and larger nuclei than oligodendrocytes and microglia, show fibrils in their cytoplasm and can have either a round, oval or irregular nucleus (Pannese, 2014, p. 199). We also assumed, that if a cell nucleus is in proximity of a blood vessel, the cell is more likely to be an astrocyte because these cells make up part of the blood-brain-barrier (Fig. 2).

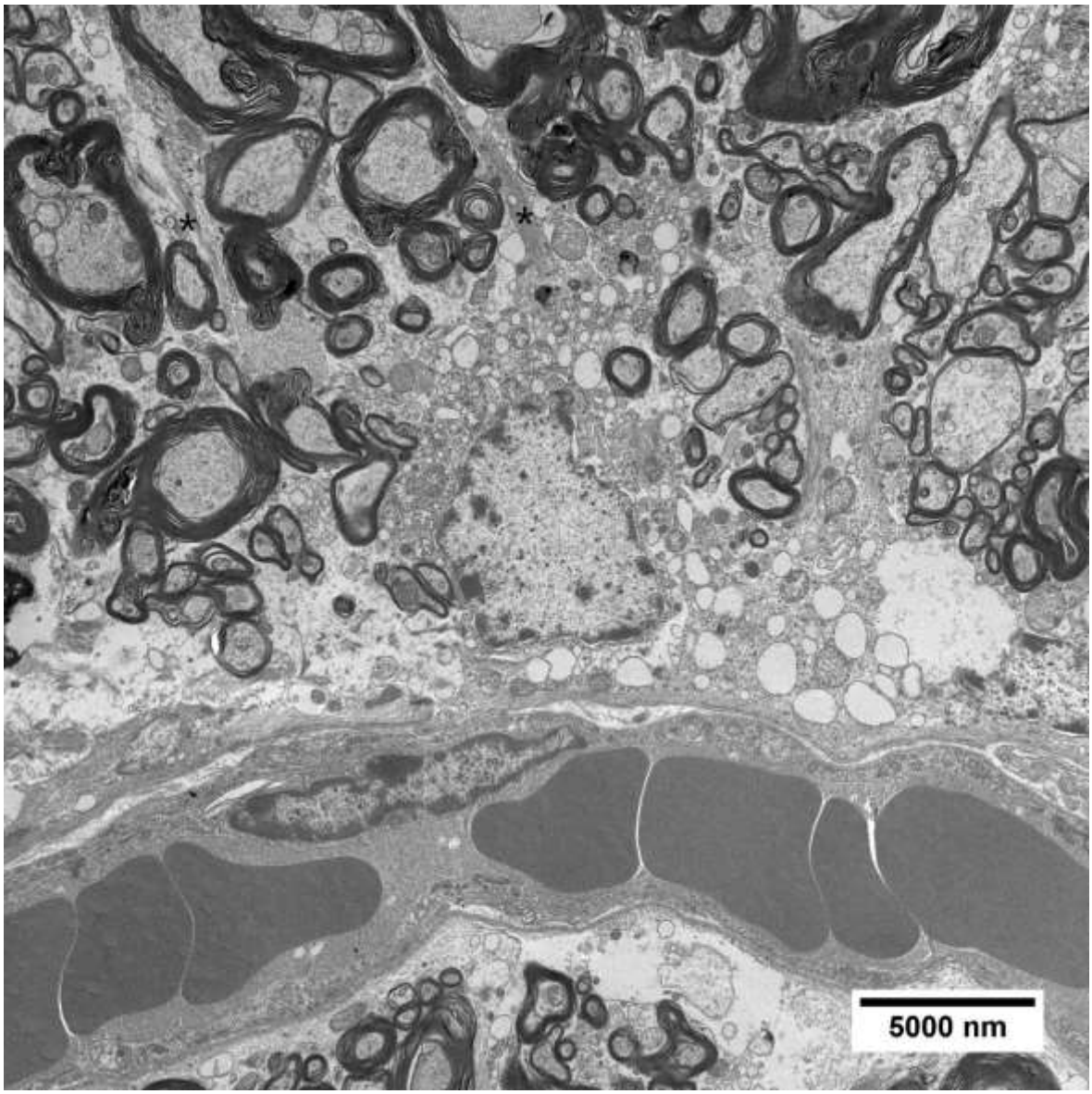

Fig. 2 Fibrous astrocyte at 12 h post-mortem on top of a capillary (3000x). The star shaped appearance of the astrocytes is seen by its radiant arms (*) on the top left of the picture.

Compared to astrocytes, oligodendrocytes are smaller and have smaller nuclei as well as a spherical (polyhedral) body (Pannese, 2014, p. 213). The cytoplasm of oligodendrocytes is denser than that of astrocytes, they have more ribosomes, numerous microtubules, a low number of intermediate fibrils and many dense bodies (Pannese, 2014, p. 185). Because oligodendrocytes produce myelin, we also assumed that they are more commonly found near axons than astrocytes (Fig. 3).

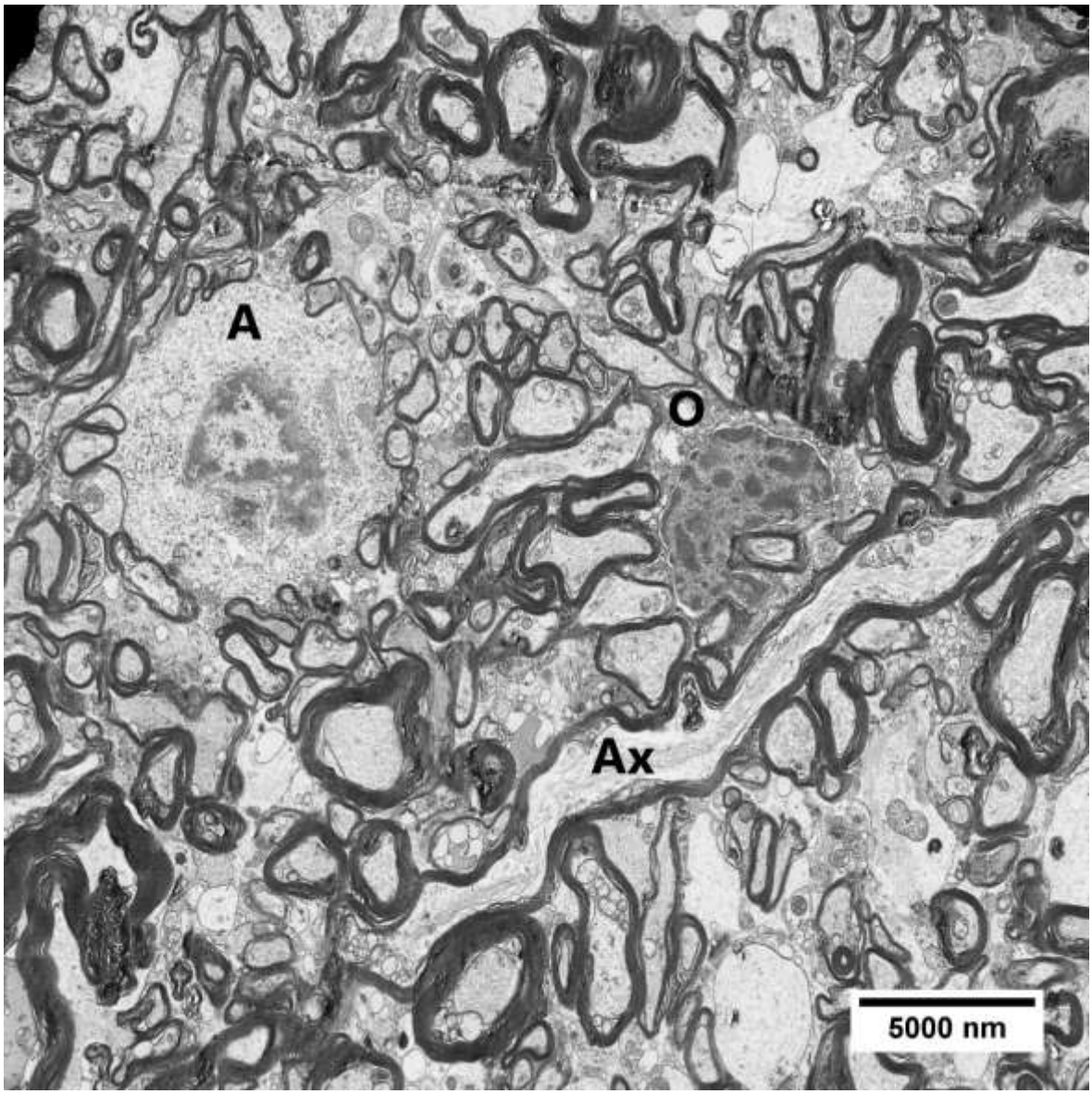

Fig. 3 Left astrocyte (A), right oligodendrocyte (O) (3000x). Proximity of oligodendrocyte to axon (Ax) visible. Astrocyte soma bigger than oligodendrocyte cell body. Cytoplasm of astrocyte (left) is far less dense, than that of the oligodendrocyte.

We also used the above-mentioned criteria to distinguish astrocytes from oligodendrocytes in grey matter grids.

Nuclei of neurons are spherical or ellipsoidal in shape, but can also be completely irregular (Pannese, 2014, p. 56). Also, the nuclear volume is usually proportional to the neuronal size (Pannese, 2014, p. 56). The axon hillock of a neuron is a conical region of the perikaryon which can contain free polysomes, mitochondria, microtubules, neurofilaments, and a few cisternae of the granular endoplasmic reticulum, which are visible in electron microscopy (Pannese, 2014, p. 75). Also, microtubules and neurofilaments funnel into the initial segment of the axon of a neuron without interruption (Pannese, 2014, p. 75).

3 Results

We investigated the post-mortem ultrastructural changes of 17 frontal lobe neurons (of which 8 were pyramid cells), 18 astrocytes and 16 oligodendrocytes (51 cells overall) in a post-mortem- interval (PMI) of 0 h, 3 h, 6 h and 12 h.

3.1 Ultrastructural changes in the post-mortem interval

3.1.1 0 h

Concerning chromatin condensation, there are only a few cells, all of which are pyramidal cells, that show no chromatin condensation at all (Fig. 5). All other cells, be it astrocytes, oligodendrocytes or neurons, show all the same nuclear changes as shown in Fig. 4.

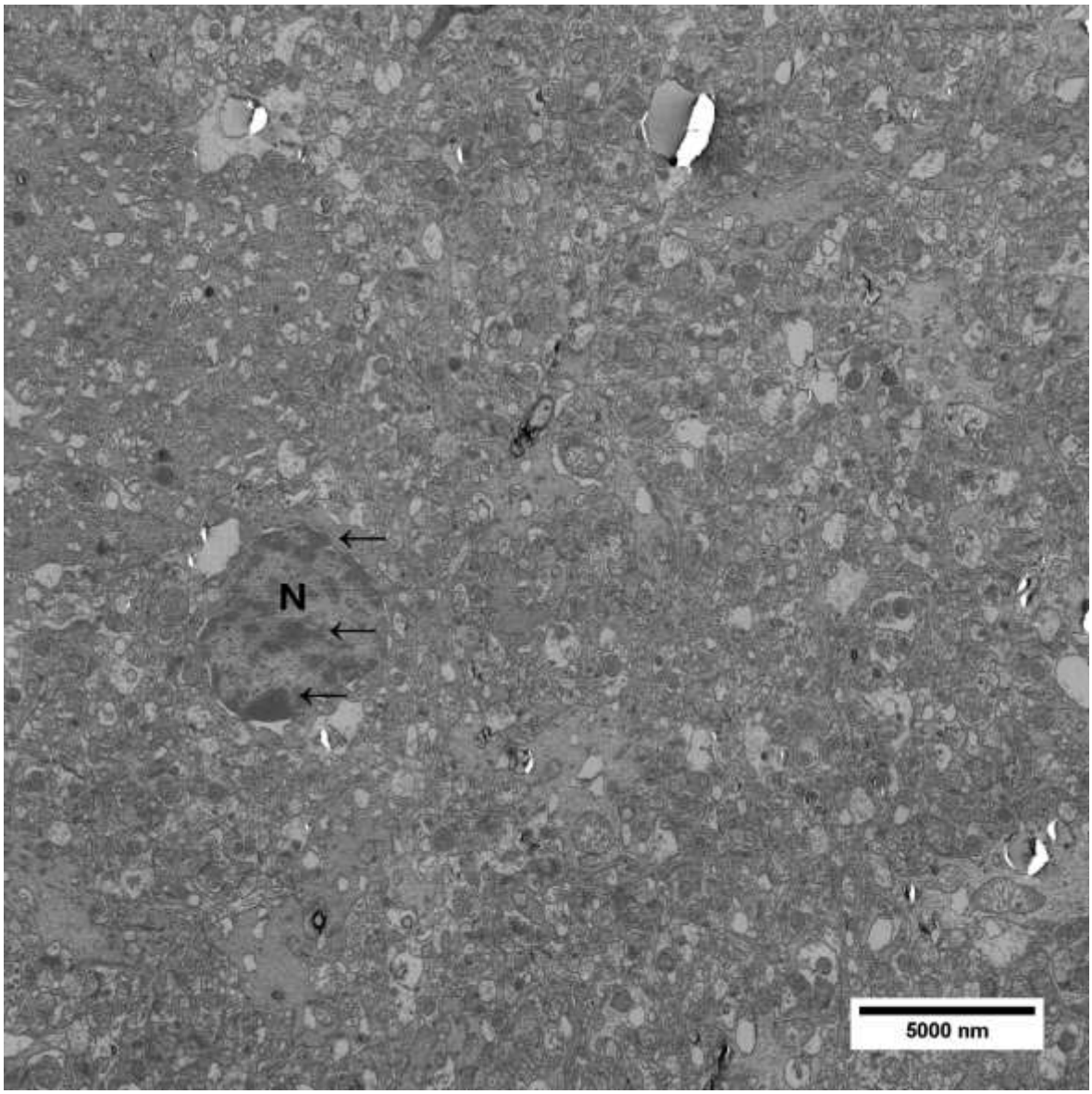

Fig. 4 Neuron at 0 h post-mortem (3000x). The nucleus (N) shows clear loci of chromatin clumps (arrows) which are characteristic for chromatin condensation.

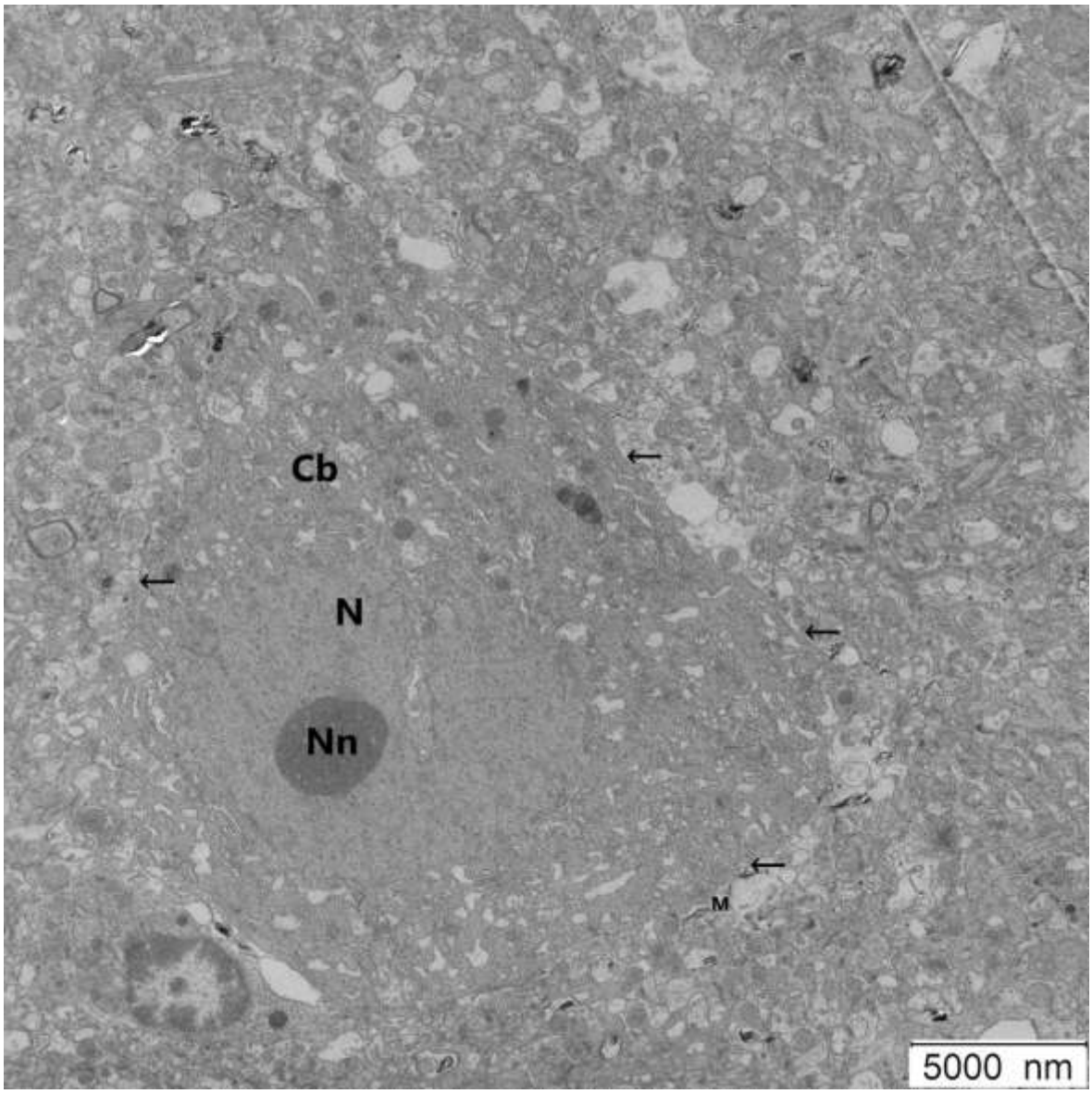

Fig. 5 Pyramid cell (neuron) body at 0 h post-mortem (3000x). Compared to non-pyramid cell neurons, pyramid cells have a bigger nucleolus (Nn) in their nucleus (N), as well as a bigger cell body (Cb). The arrows show the cell margins of the pyramid cell. Also, there is no clear condensation of chromatin recognizable in this image. M = mitochondria.

At 0 h post-mortem there were no cells with obvious intracytoplasmic vacuolization, as well as no cells matching our criteria for unphysiological ER. Although a lot of the ER happened to be more circular than ovoid in shape, none of our cells showed solely smooth ER. An example is shown in Fig. 6 and Fig. 7.

The mitochondria looked normal in all the investigated cells at 0 h post-mortem.

Regarding the lysosomes, autophagosomes and autolysosomes, we only found lysosomes and autolysosomes at 0 h (Fig. 6 and Fig. 7).

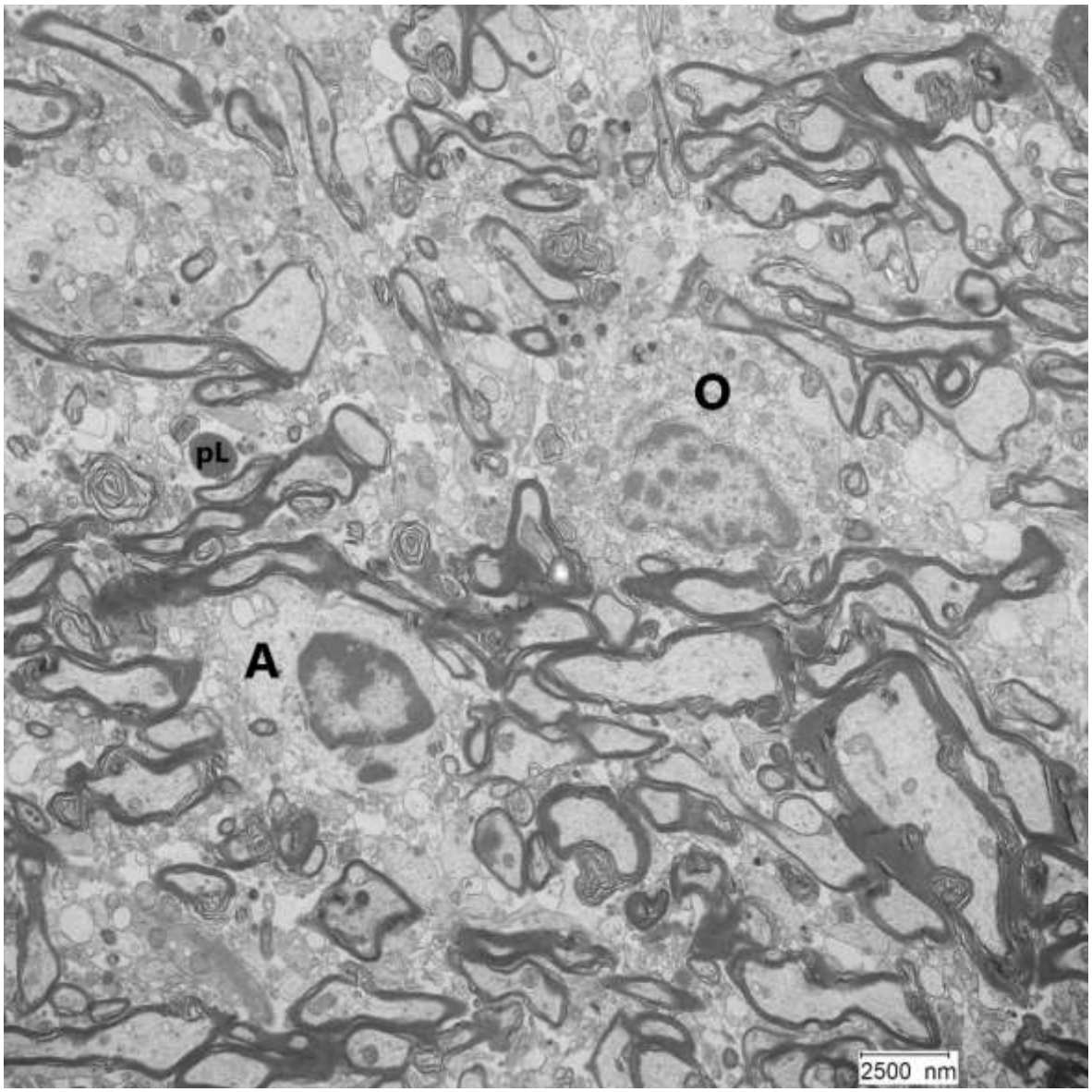

Fig. 6 Astrocyte (A) and oligodendrocyte (O) at 0 h post-mortem (3000x). Both cells show strong chromatin condensation as well as different densities in their cytoplasm (astrocyte has lighter cytoplasm than oligodendrocyte). Criteria for unphysiological ER not met. We also found a primary lysosome (pL) in this picture.

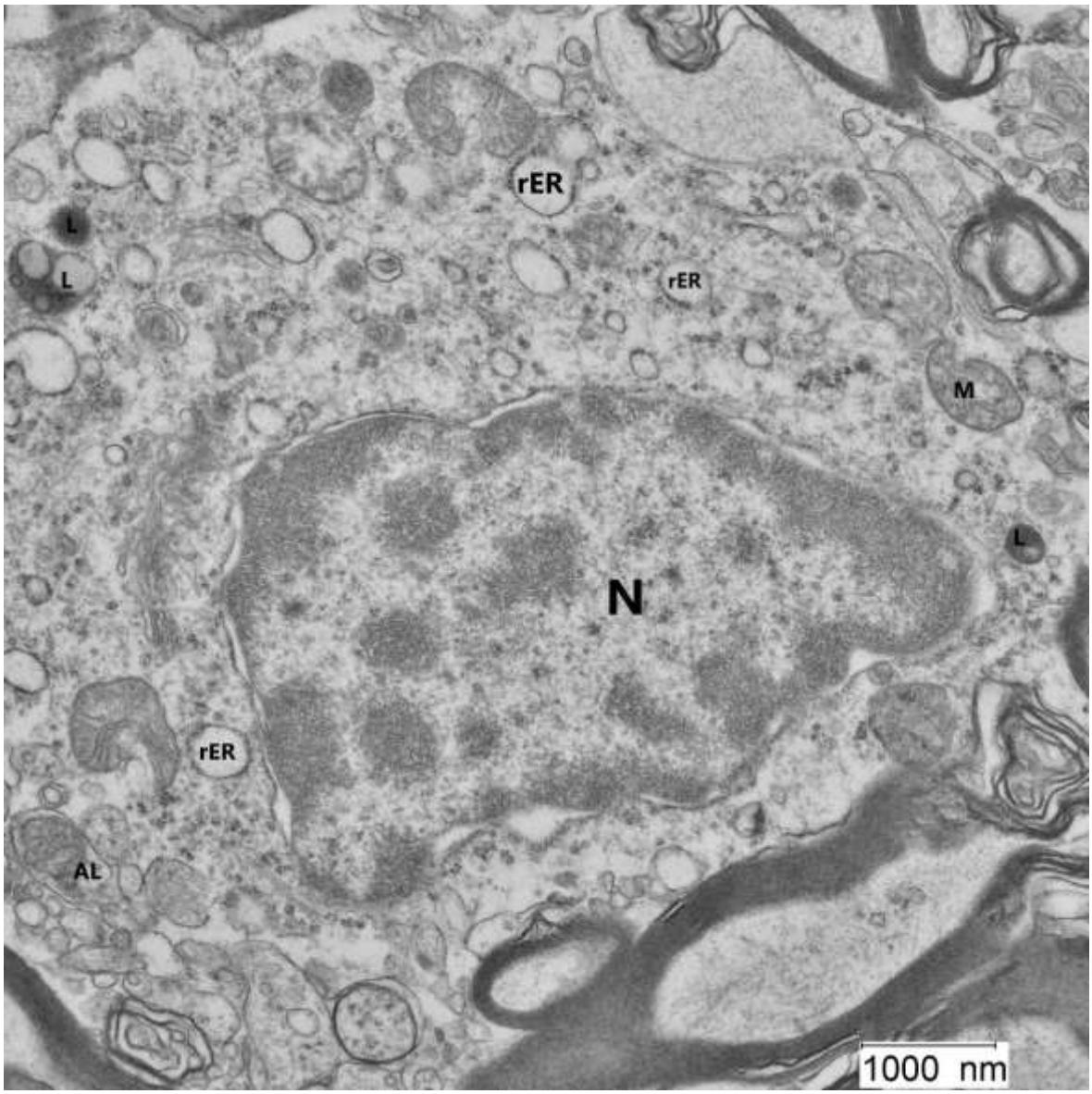

Fig. 7 Oligodendrocyte at 0 h post-mortem (12000x). This image shows the nucleus (N) of an oligodendrocyte with ribosome-containing ER (rER), lysosomes (L), an autolysosome (AL) and some mitochondria (M).

3.1.2 3 h

At the next point in time, we again investigated chromatin condensation. Now, 100 % of the cells showed this autolytic change, including pyramid cells (Fig. 8)

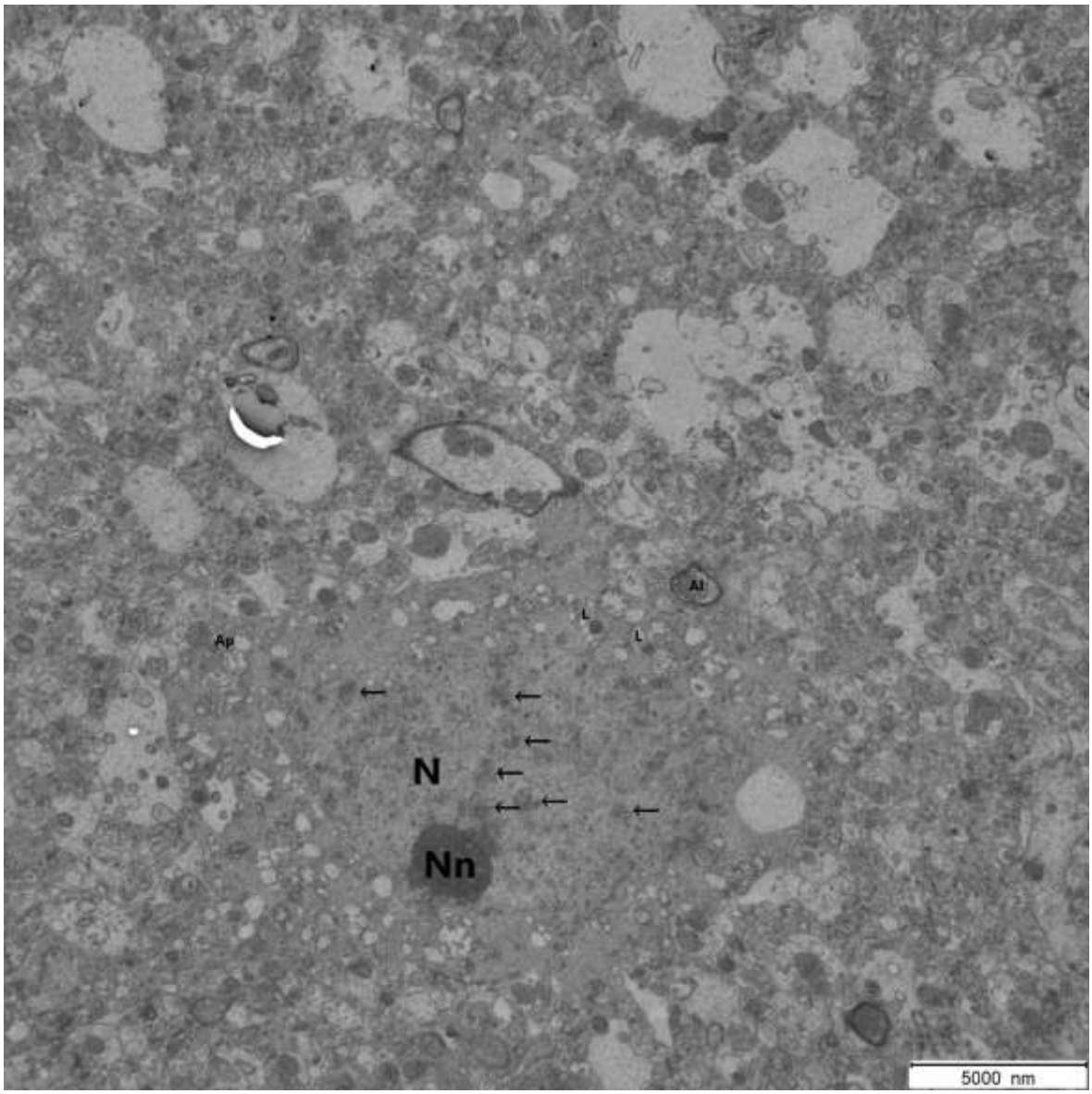

Fig. 8 Pyramid cell body at 3 h post-mortem (3000x). Here we see chromatin clumps (arrows) in the nucleus (N), and nearby the nucleolus (Nn). Also, in the left side of the pyramid cell, there is an autophagosome (Ap) and on the right-side an autolysosome (Al) and a few lysosomes (L). All mitochondria in this image show structural deficits.

The first time intracytoplasmic vacuolization took place, was at 3 h post-mortem (Fig. 9).

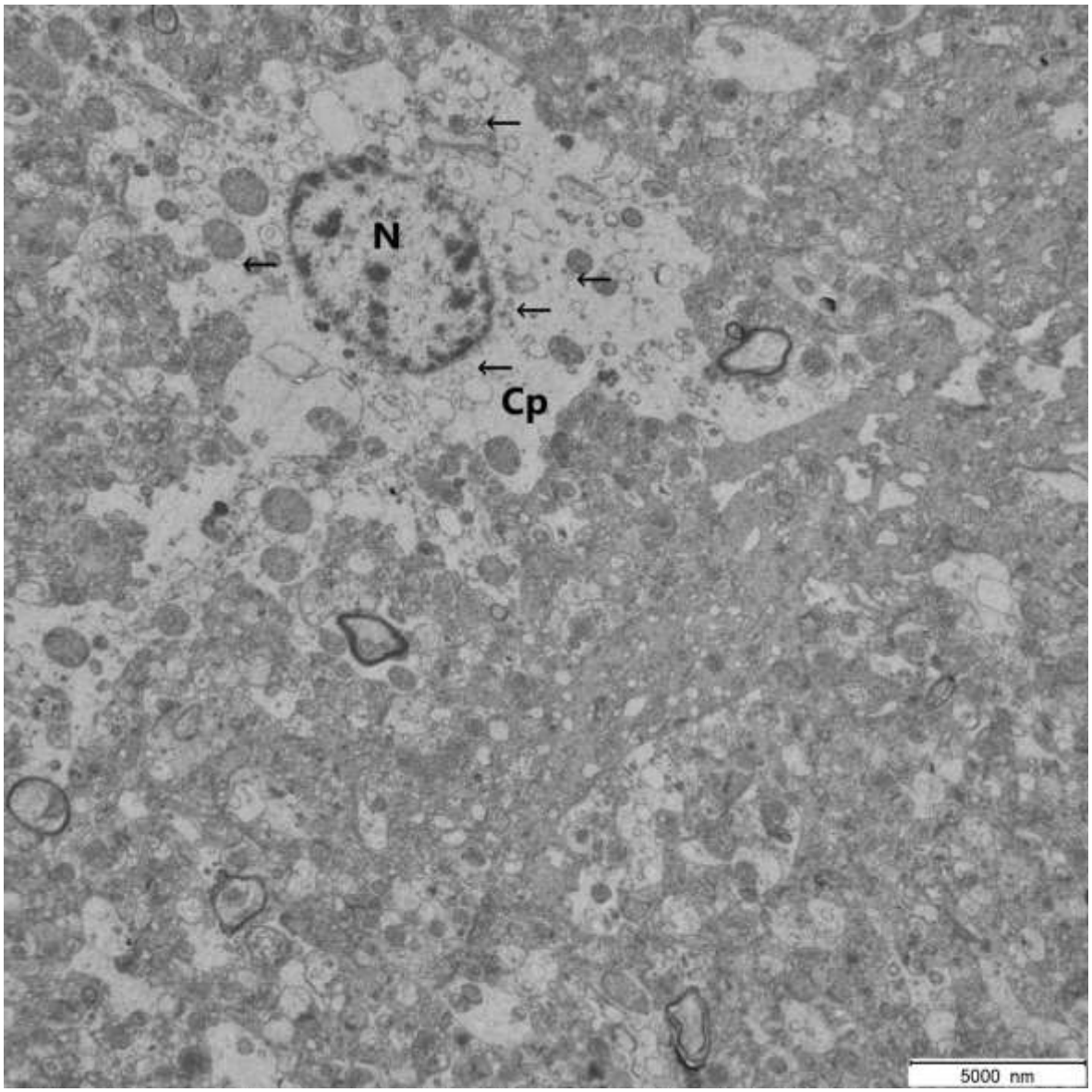

Fig. 9 Astrocyte at 3 h post-mortem (3000x). In this image we see highly lysed cytoplasm (Cp) with many small intracytoplasmic vacuoles (arrows) around the nucleus (N).

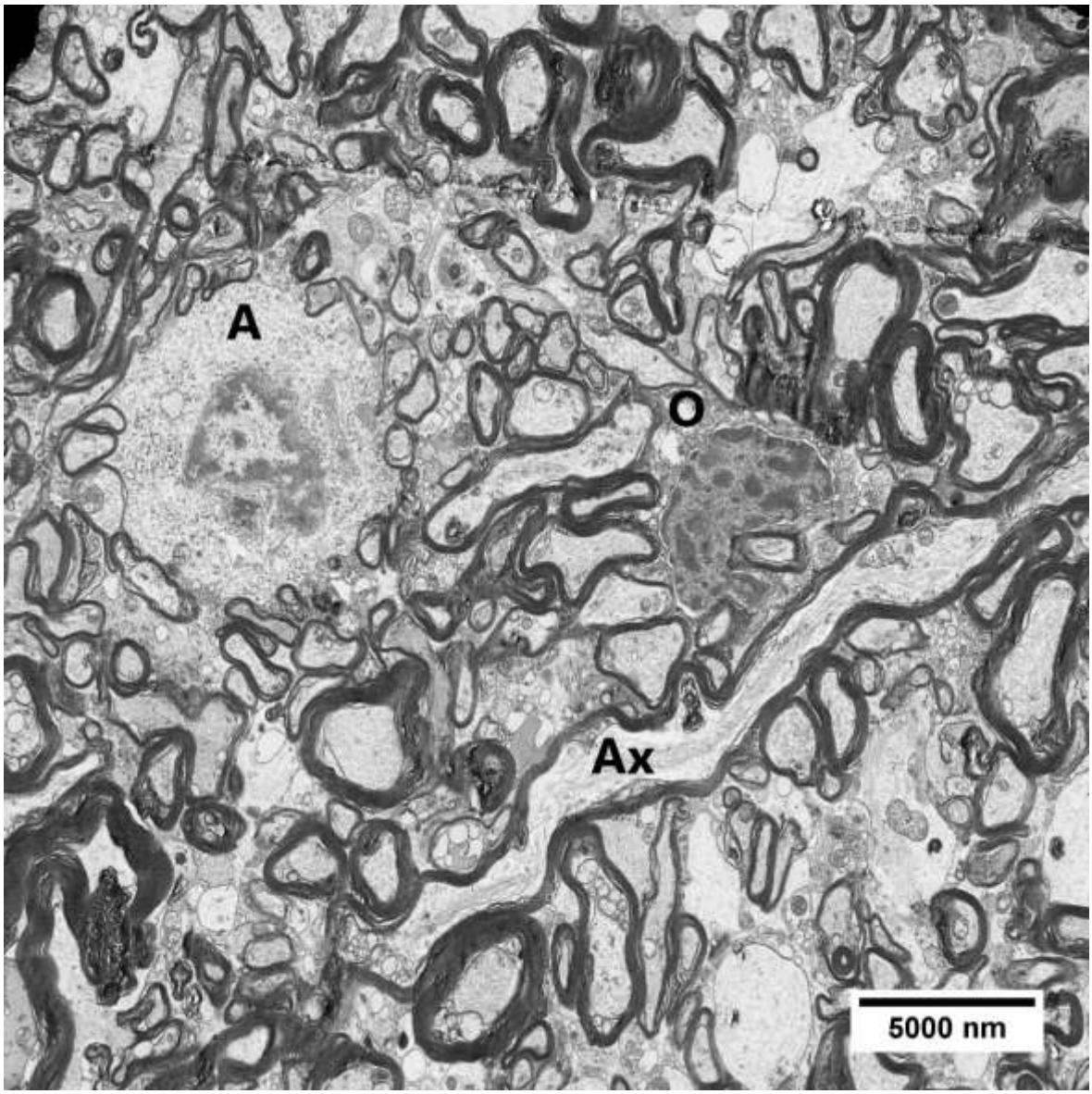

Fig. 10 Astrocyte (A) and oligodendrocyte (O) at 3 h post-mortem (3000x). There are no intracytoplasmic vacuoles seen in neither the astrocyte nor the oligodendrocyte (only ER). Also, the oligodendrocyte "sits" on a longitudinally cut axon (Ax) of a neuron.

We also found one neuron that met our criteria regarding unphysiological ER (Fig. 11 and Fig. 12).

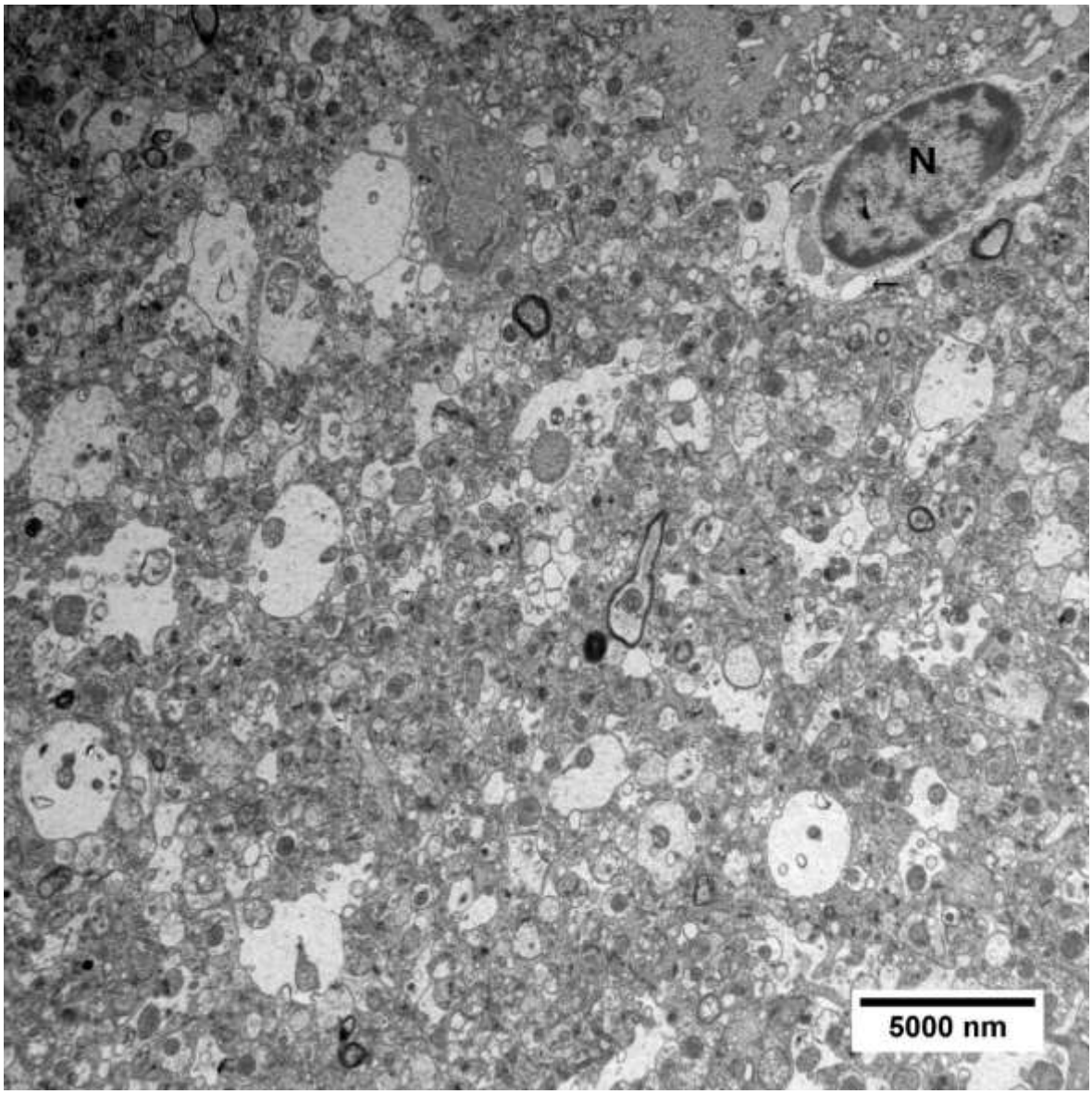

Fig. 11 Neuron at 3 h post-mortem (3000x). Near the nucleus (N) is one ER without ribosomes (arrow).

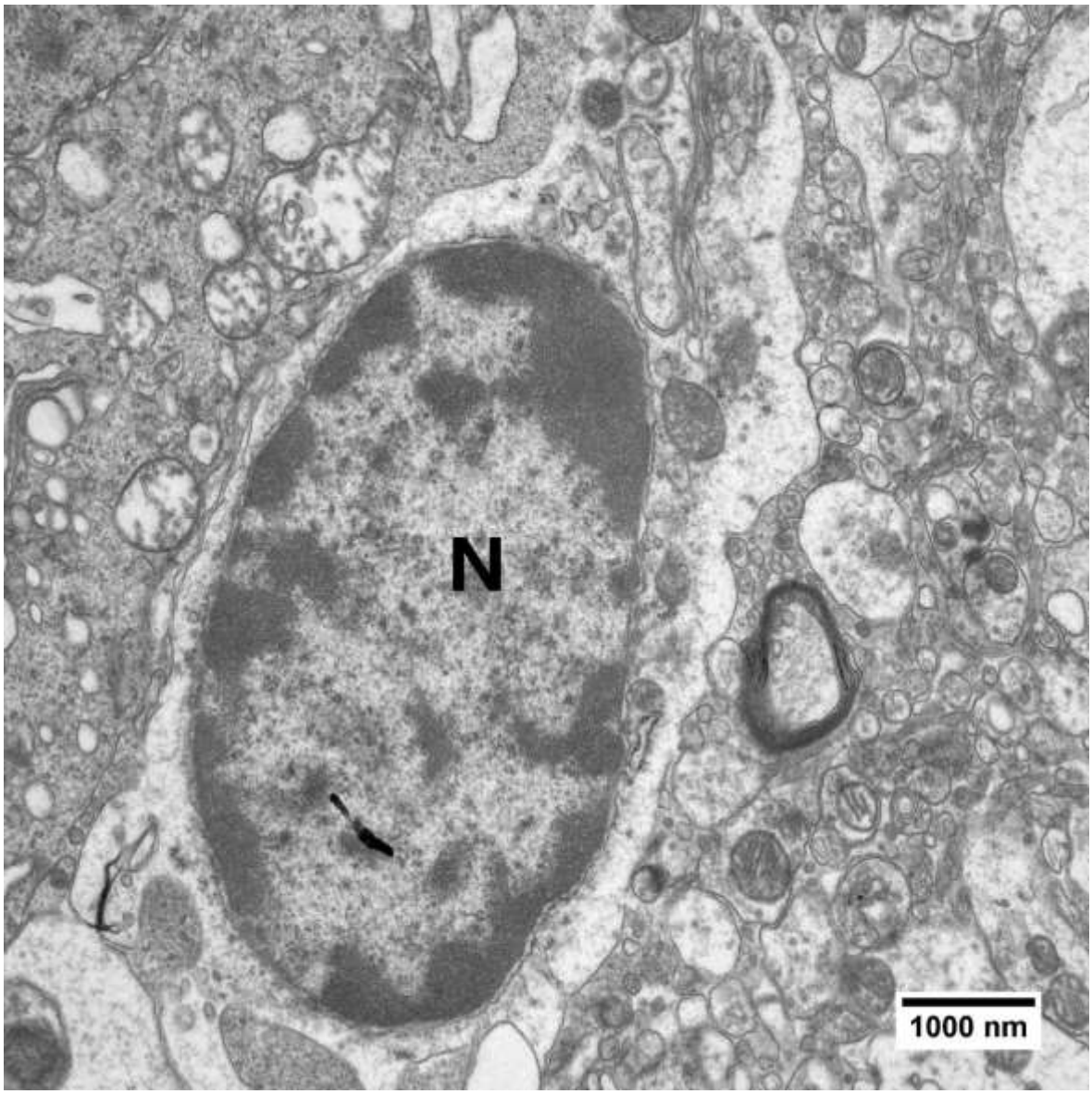

Fig. 12 Neuron at 3 h post-mortem (12000x). Near the nucleus (N) is the half of an ER without ribosomes.

Nearly all mitochondria showed normal ultrastructure at 3 h post-mortem except for mitochondria in one picture (Fig. 8).

We found all autolytic organelles including lysosomes, autophagosomes and autolysosomes in different numbers of cells (Fig. 8).

3.1.3 6 h

At 6 h post-mortem chromatin condensation occurred at 100 % of all cells.

The intracytoplasmic vacuolization took place in over the half of the cells investigated (Tab. 4, Fig. 13 and Fig. 14).

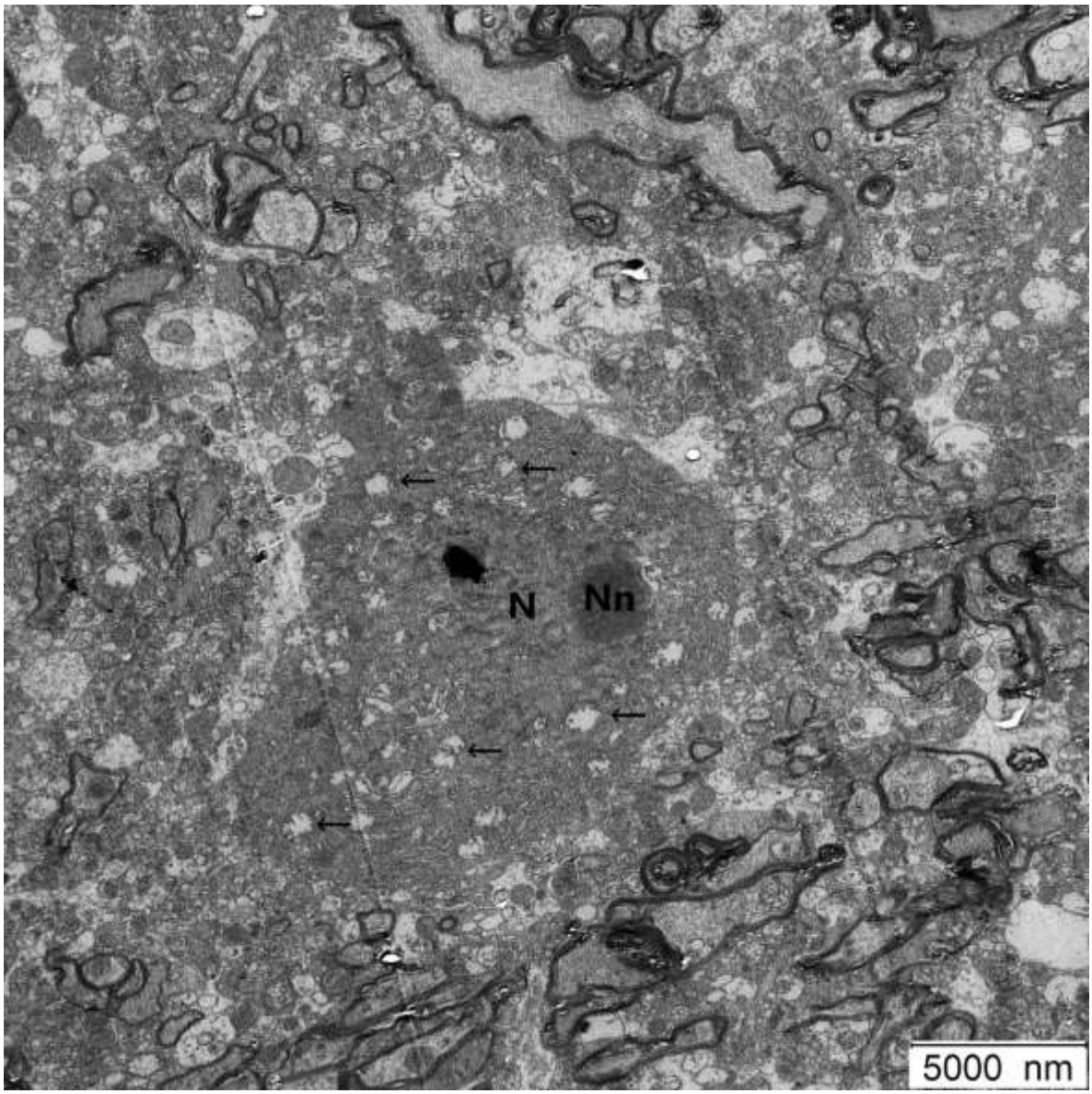

Fig. 13 Pyramid cell body at 6 h post-mortem (3000x). We see many intracytoplasmic vacuoles (arrows) around the nucleus (N) and inside the cell body. Nn = nucleolus.

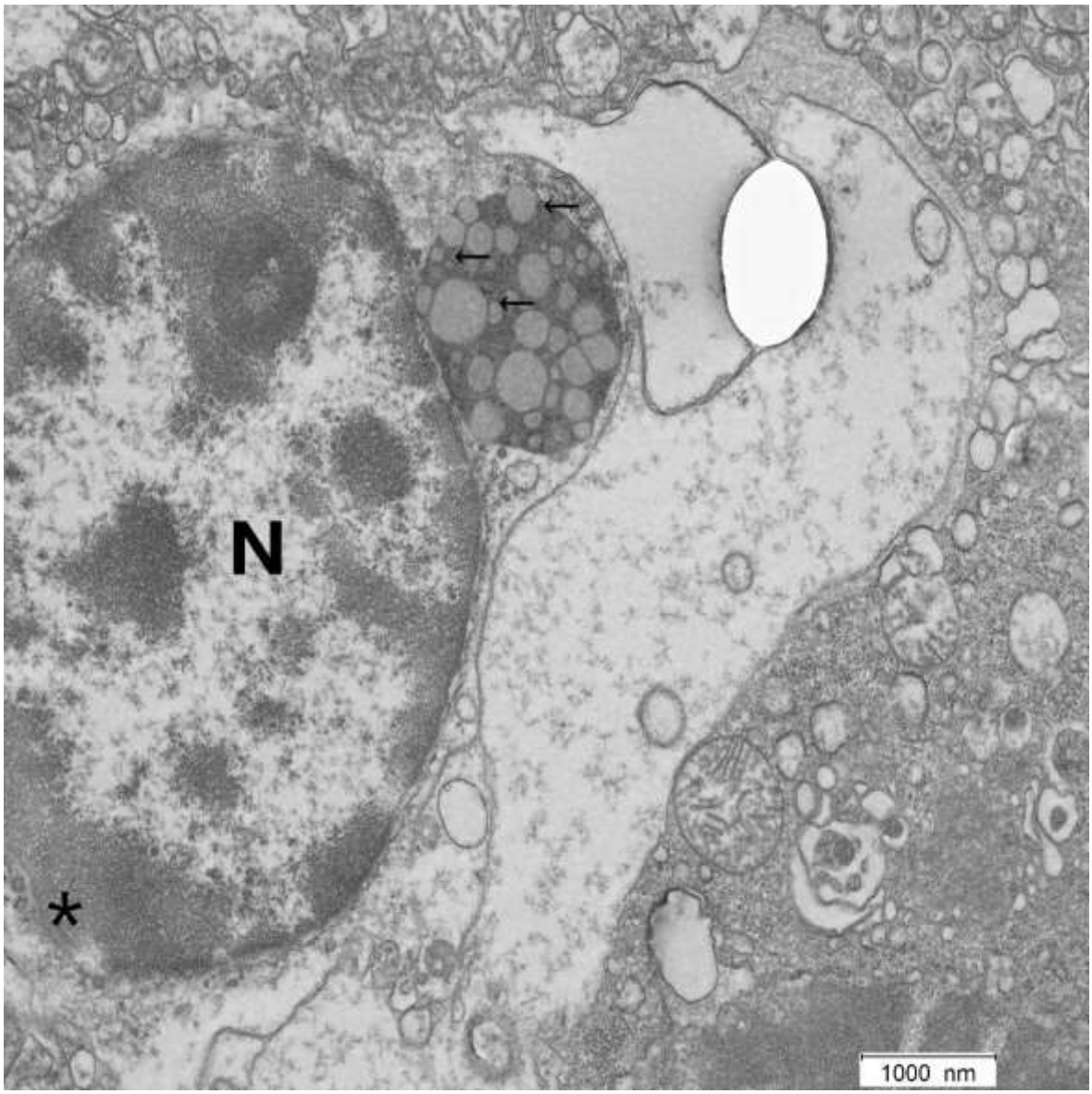

Fig. 14 Oligodendrocyte at 6 h post-mortem (12000x). There is a dense organelle containing multiple vacuoles (arrows) near the nucleus (N). Also, the nucleolar membrane is lytic (*), which is an indicator for karyolysis.

The ER of none of the frontal lobe cells matched our criteria for unphysiological ER. We found many lysosomes at 6 h post-mortem (Fig. 16 and Fig. 18) as well as autophagosomes (Fig. 18), but no autolysosomes.

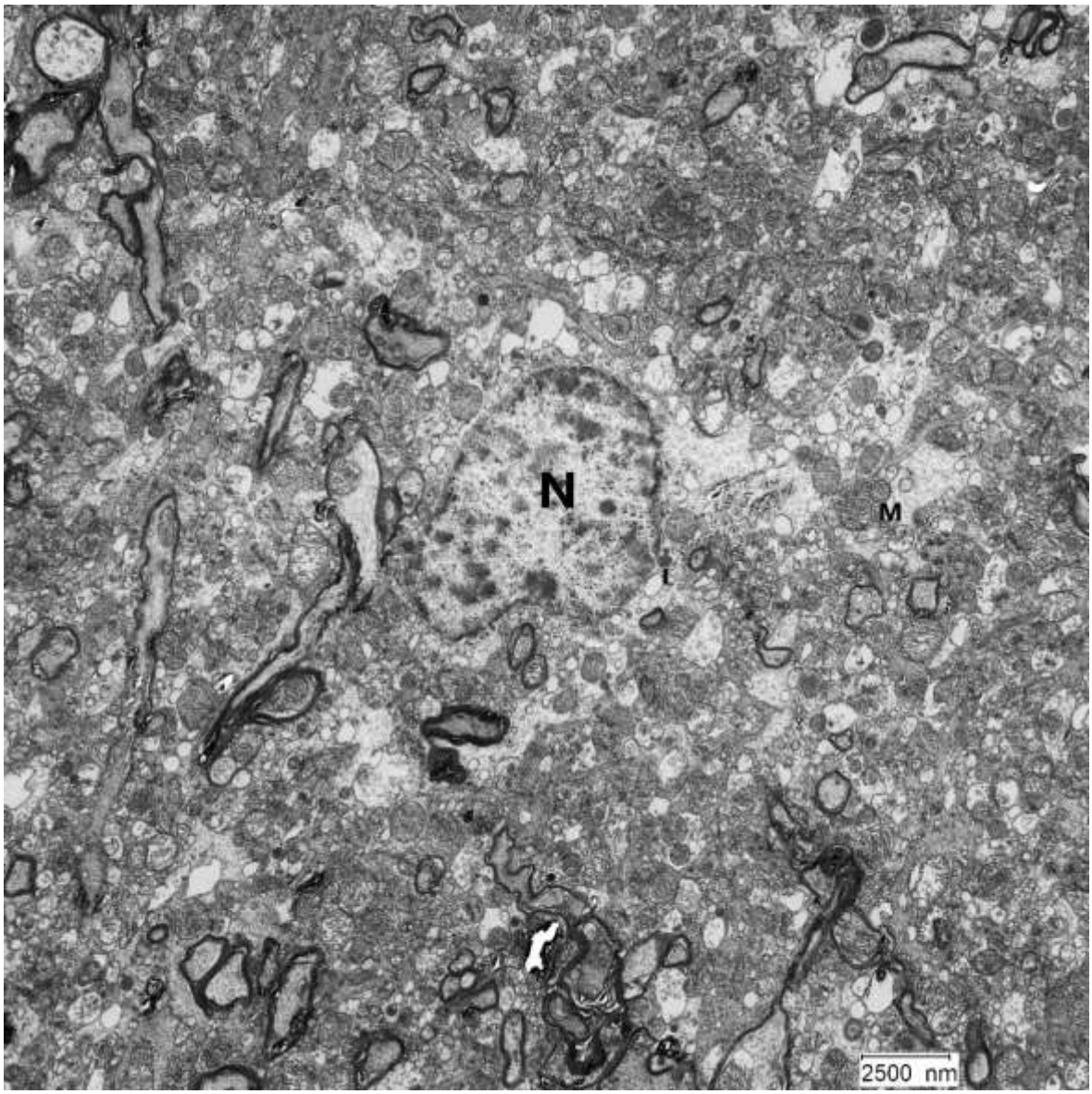

Fig. 15 Neuron at 6 h post-mortem (3000x). N = nucleus; M = mitochondria.

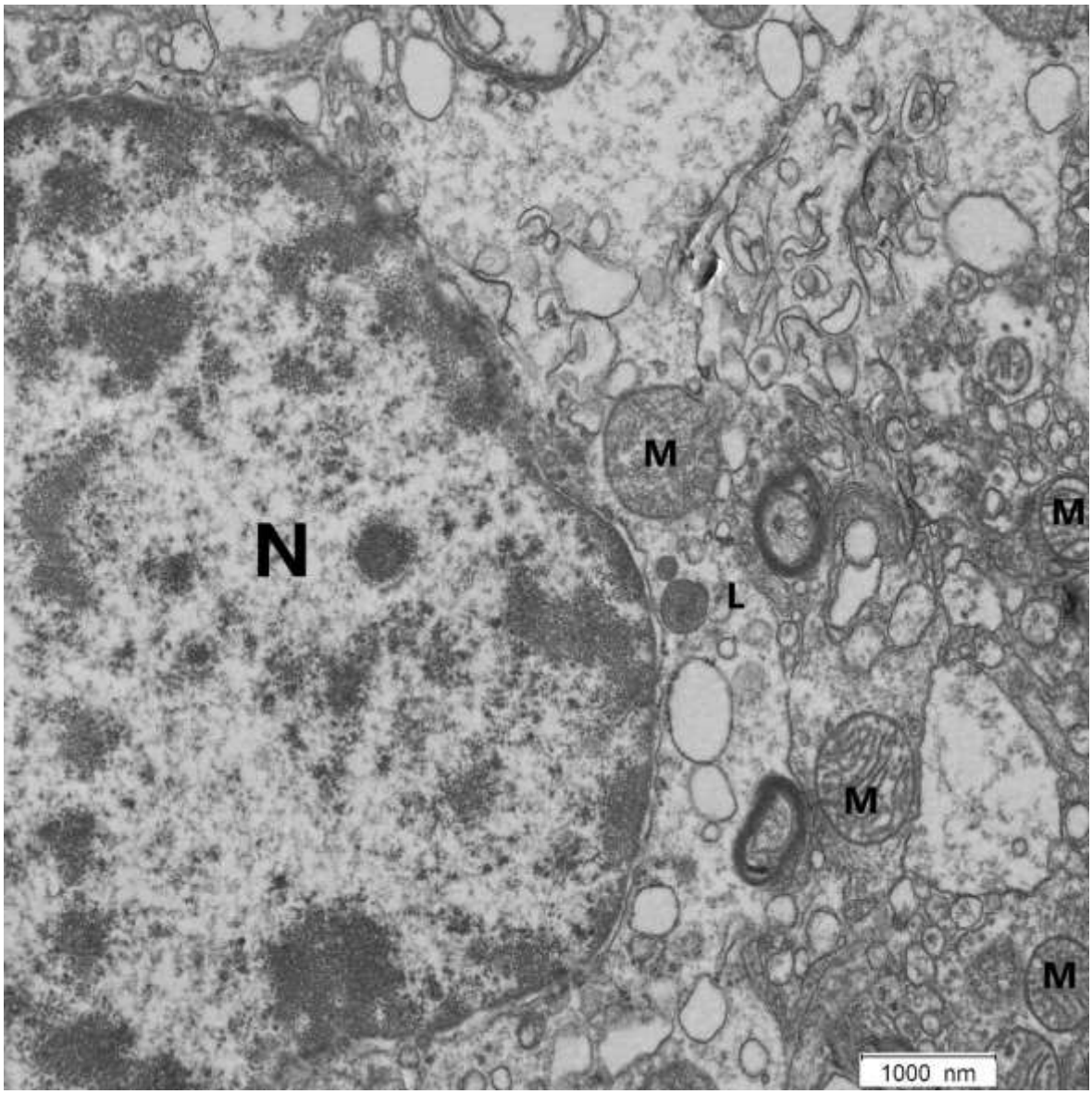

Fig. 16 Neuron at 6 h post-mortem (12000x). In this image, we see multiple mitochondria (M), which differ in their structural integrity. The one inside the cell body of the neuron seems to have defect cristae, while the other ones on the right-hand side appear to have physiological cristae and therefore a normal structure. Also, there are two lysosomes (L) near the nucleus (N).

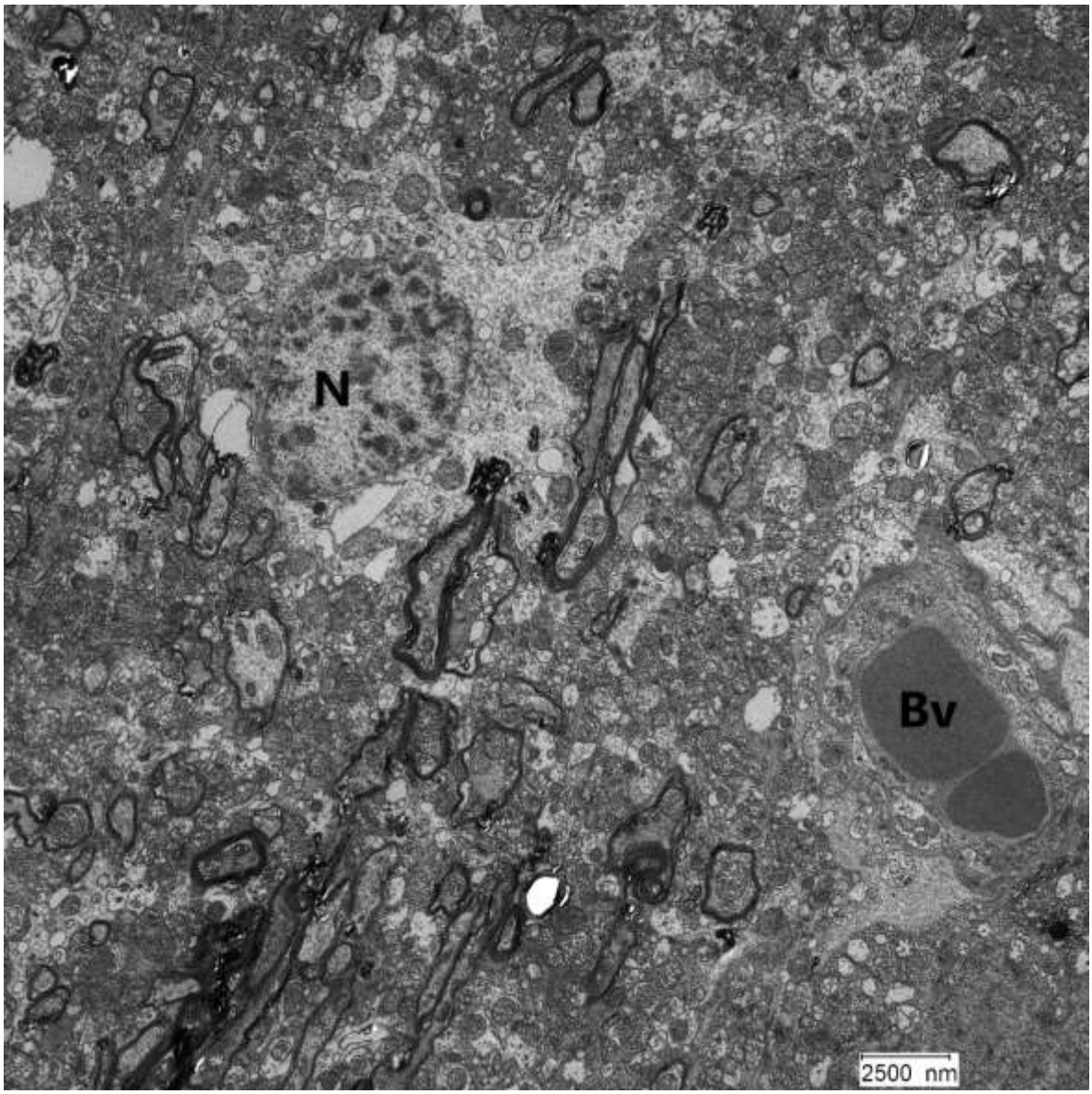

Fig. 17 Neuron at 6 h post-mortem (3000x). N = nucleus; Bv = blood vessel.

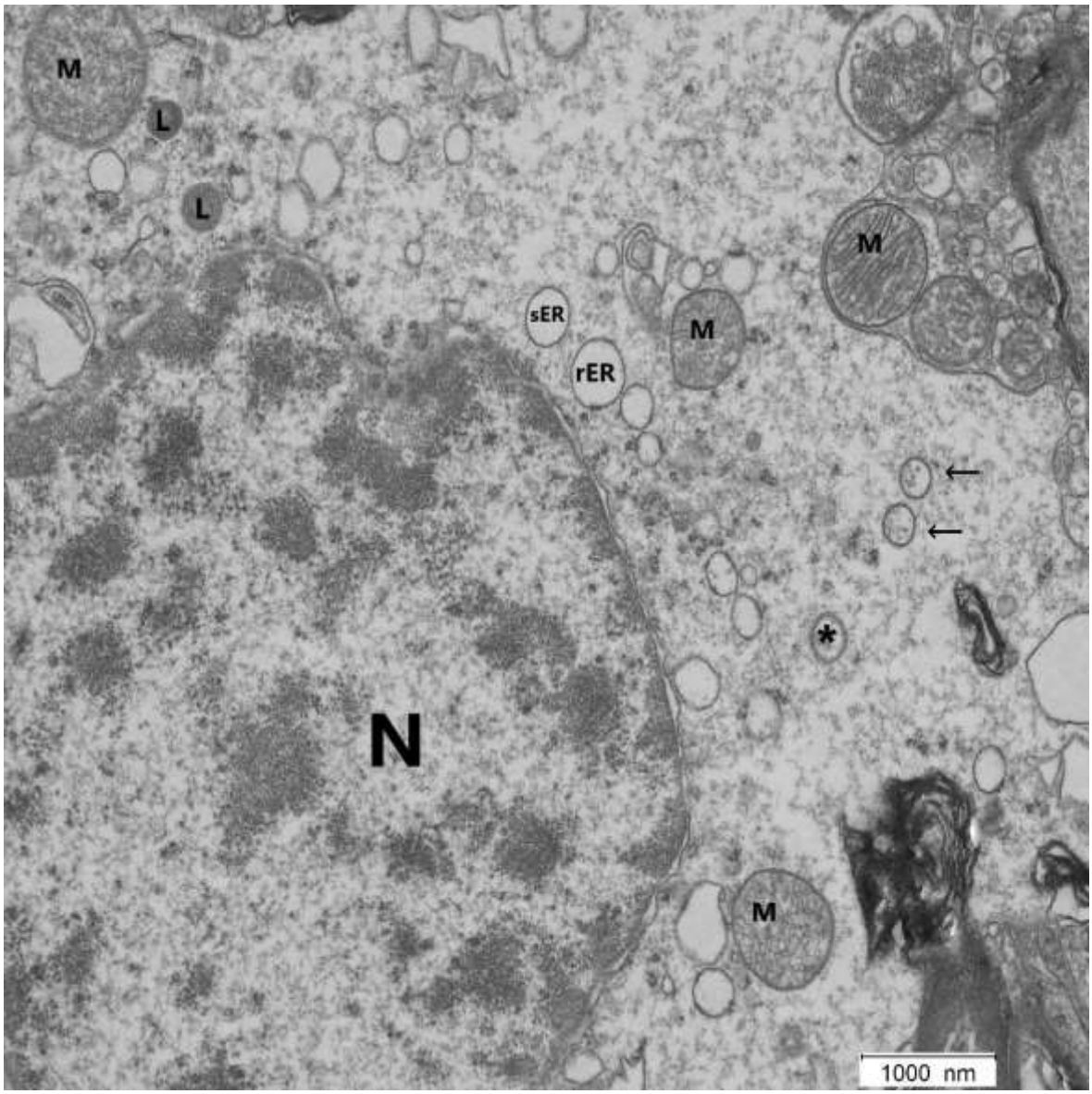

Fig. 18 Neuron at 6 h post-mortem (12000x). On the top of the nucleus, there are two lysosomes (L). Furthermore, there are two small double-membraned autophagosome (arrows) sectors seen on the right-hand side. There is also an unidentified structure (*) with a possible lysed membrane (either single- or double-membrane). The mitochondria (M) inside the cell boundaries appear to be slightly structurally damaged compared to the mitochondria outside the neuron.

3.1.4 12 h

There was 100 % chromatin condensation at 12 h post-mortem. Also, the level of condensation increased at this point in time, which is recognizable by a higher number of chromatin clumps (Fig. 19 and Fig. 20) compared to images from earlier points in time in the PMI (Fig. 4).

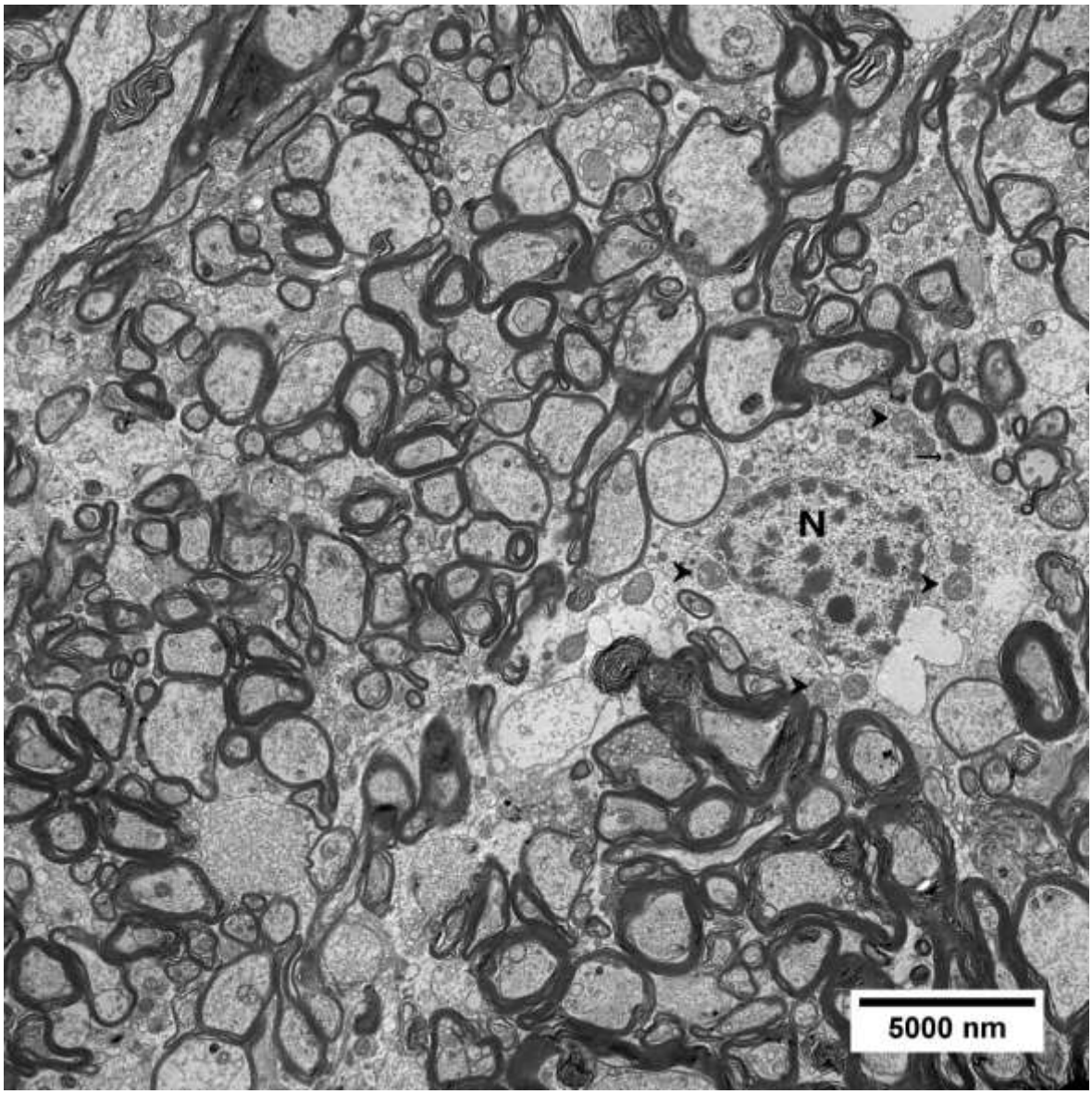

Fig. 19 Oligodendrocyte at 12 h post-mortem (3000x). There are only structurally damaged mitochondria (arrowheads) found. Also, a lysosome (arrow) is apparent in this image. N = nucleus.

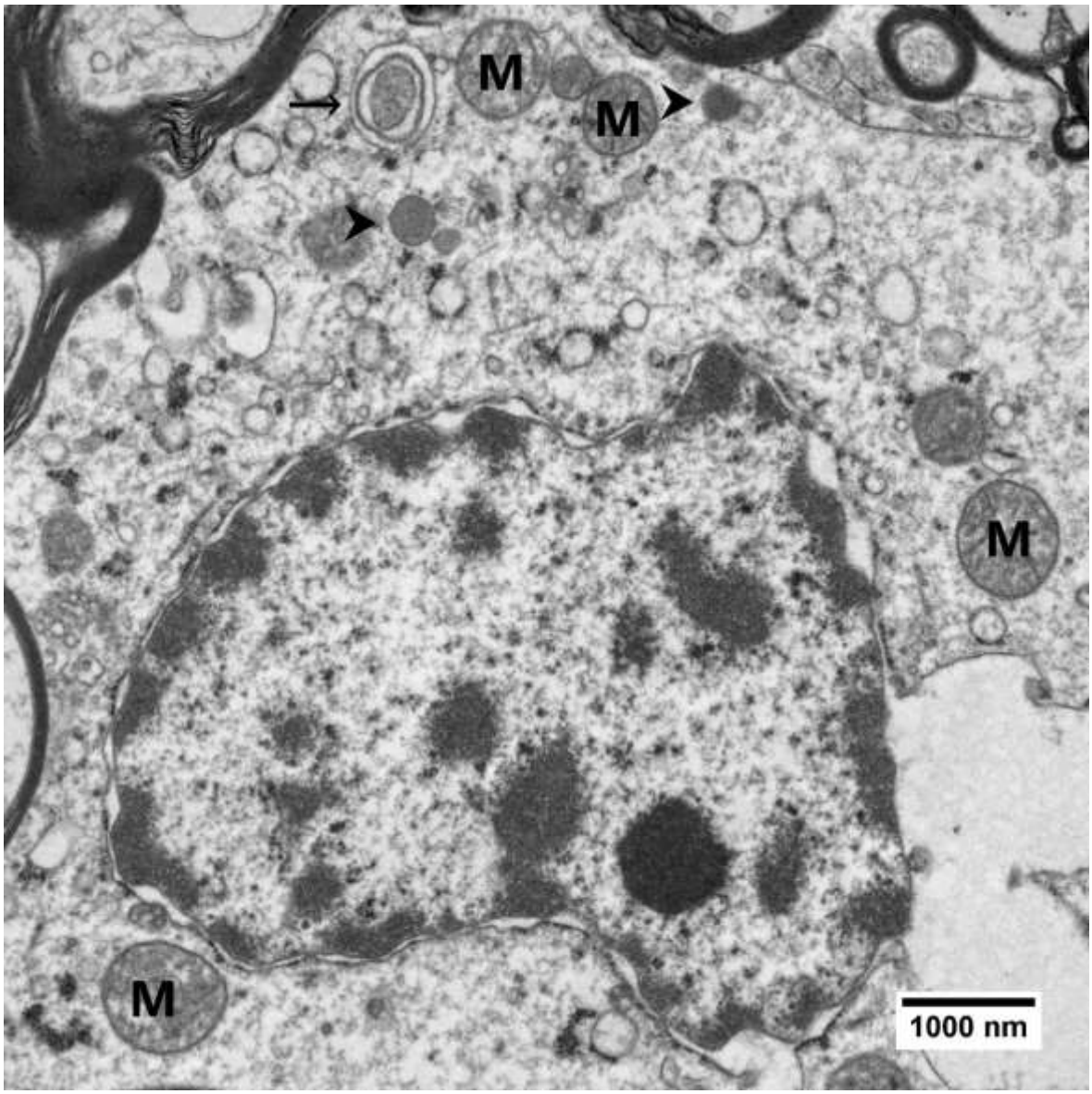

Fig. 20 Oligodendrocyte at 12 h post-mortem (12000x). Strong chromatin condensation with a high number of chromatin clumps. Also, the mitochondrial cristae of all mitochondria are damaged. There is one autophagosome (arrow) and a few lysosomes (arrowheads) apparent.

We saw strong intracytoplasmic vacuolization in some cells (Fig. 21), compared to earlier cells (Fig. 9).

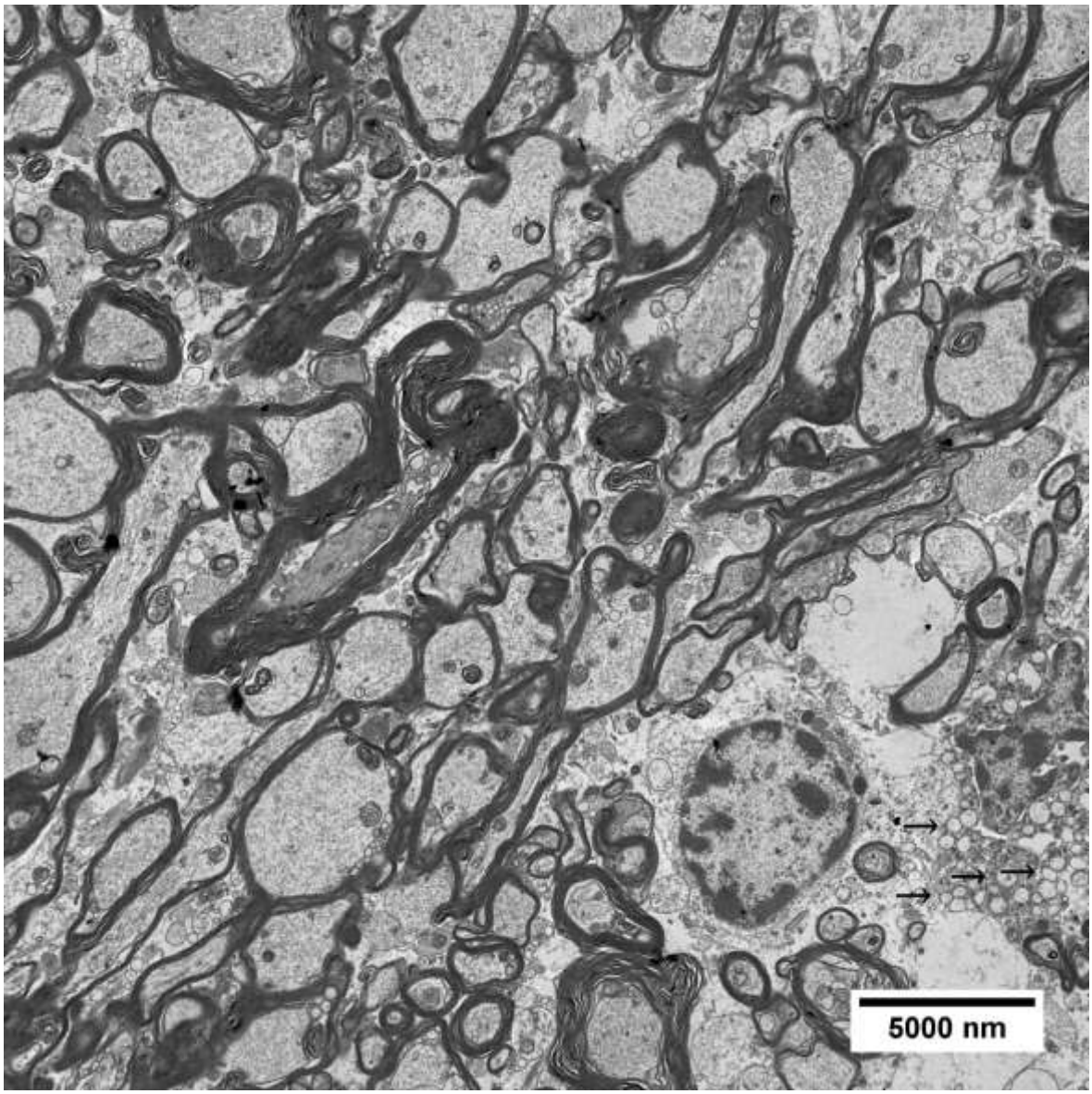

Fig. 21 Astrocyte at 12 h post-mortem (3000x). Strong intracytoplasmic vacuolization (arrows) found on the right-hand side of the image.

There were no cells matching our autolytic criteria for unphysiological ER at 12 h post-mortem.

We also found images with mitochondria showing a disintegrated structure at 12 h post-mortem (Fig. 19 and Fig. 20).

Regarding the autolytic apparatus, we found lysosomes, autophagosomes and autolysosomes (Fig. 22 - Fig. 25).

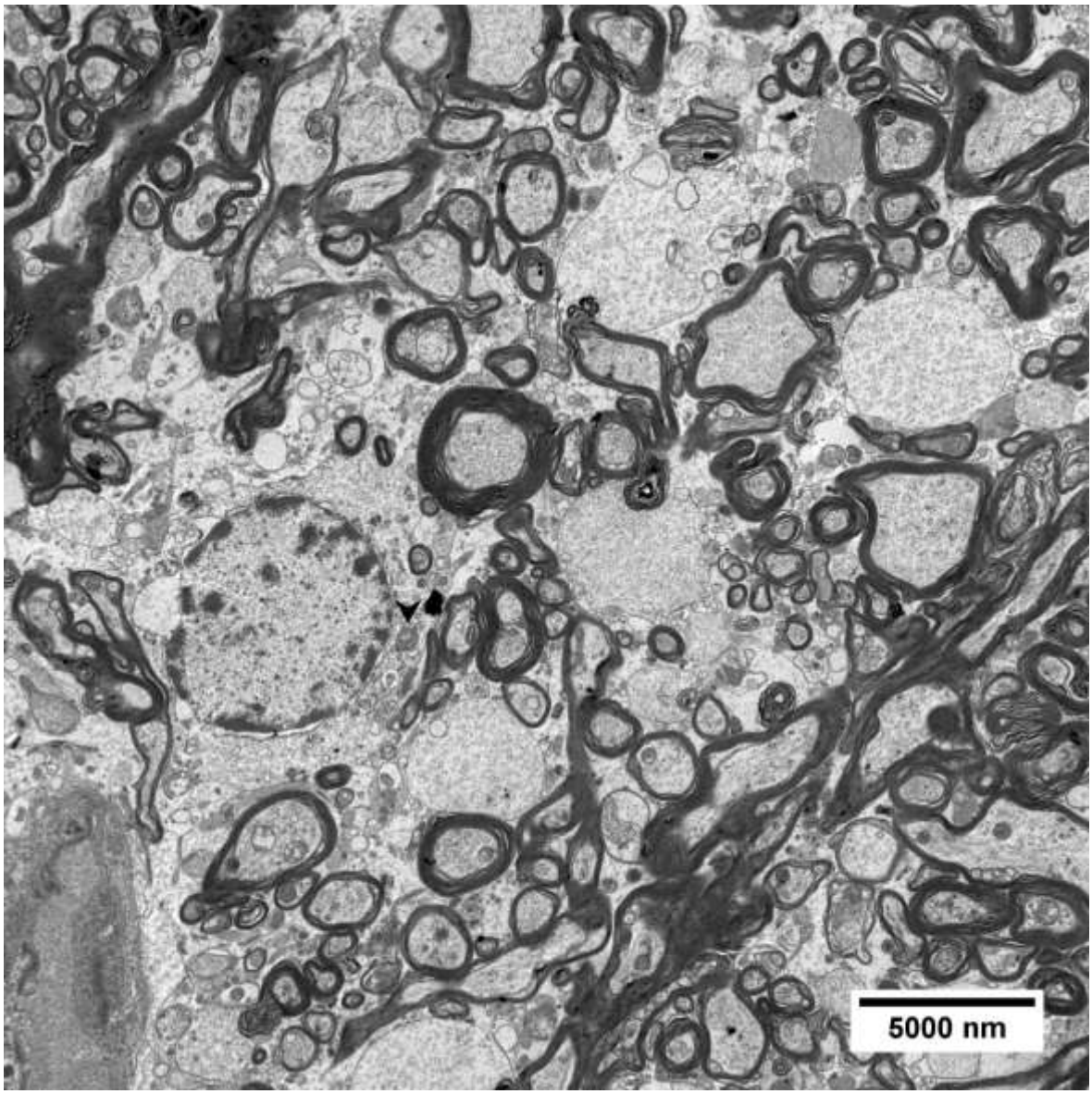

Fig. 22 Astrocyte at 12 h post-mortem (3000x). On the right-hand side of the nucleus, there is an autolysosome (arrowhead).

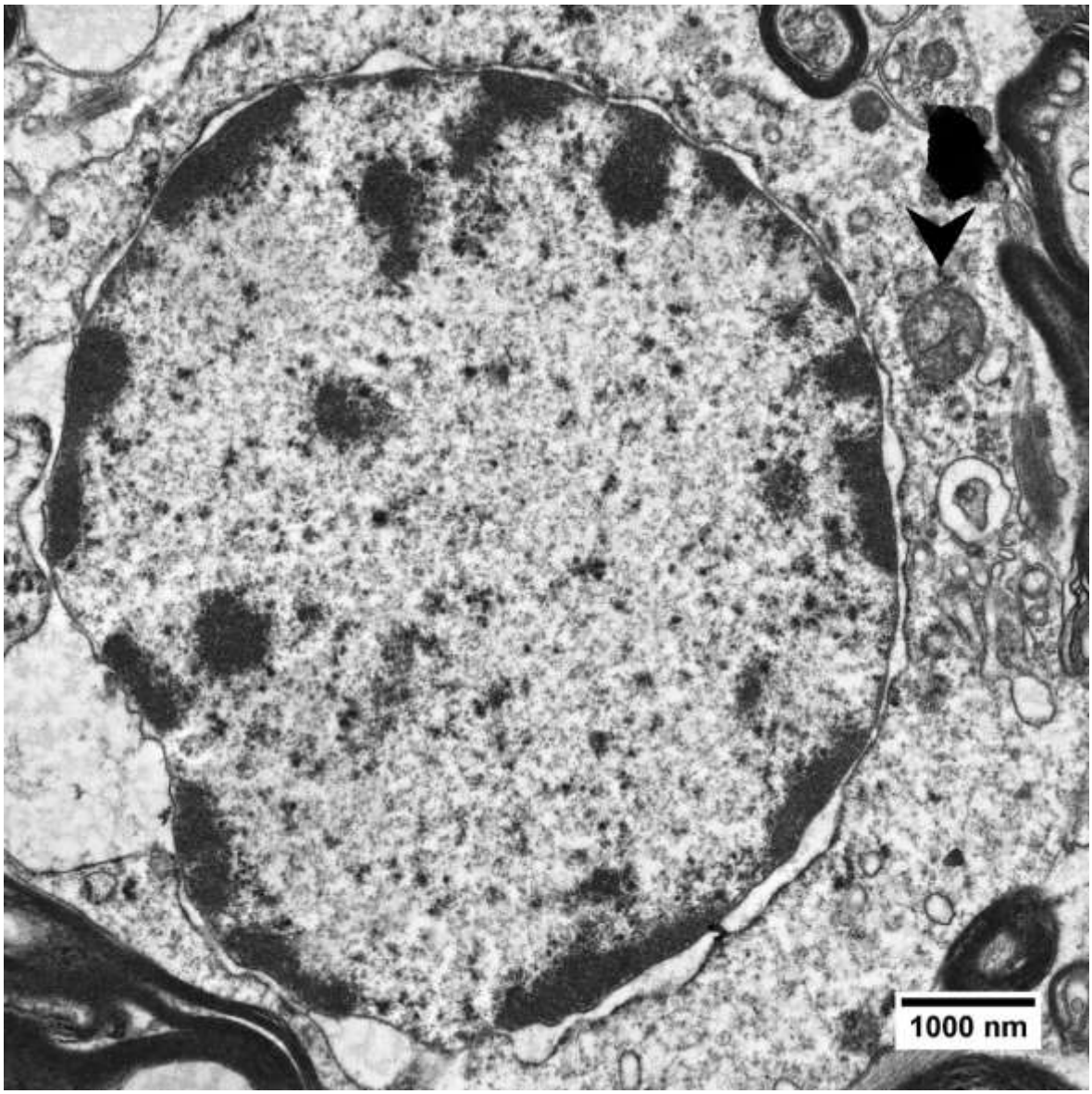

Fig. 23 Astrocyte at 12 h post-mortem (12000x). On the right-hand side of the nucleus, there is an autolysosome (arrowhead), which can be identified by the double-membrane, the density of the inside of the organelle and the two other structures engulfed in it.

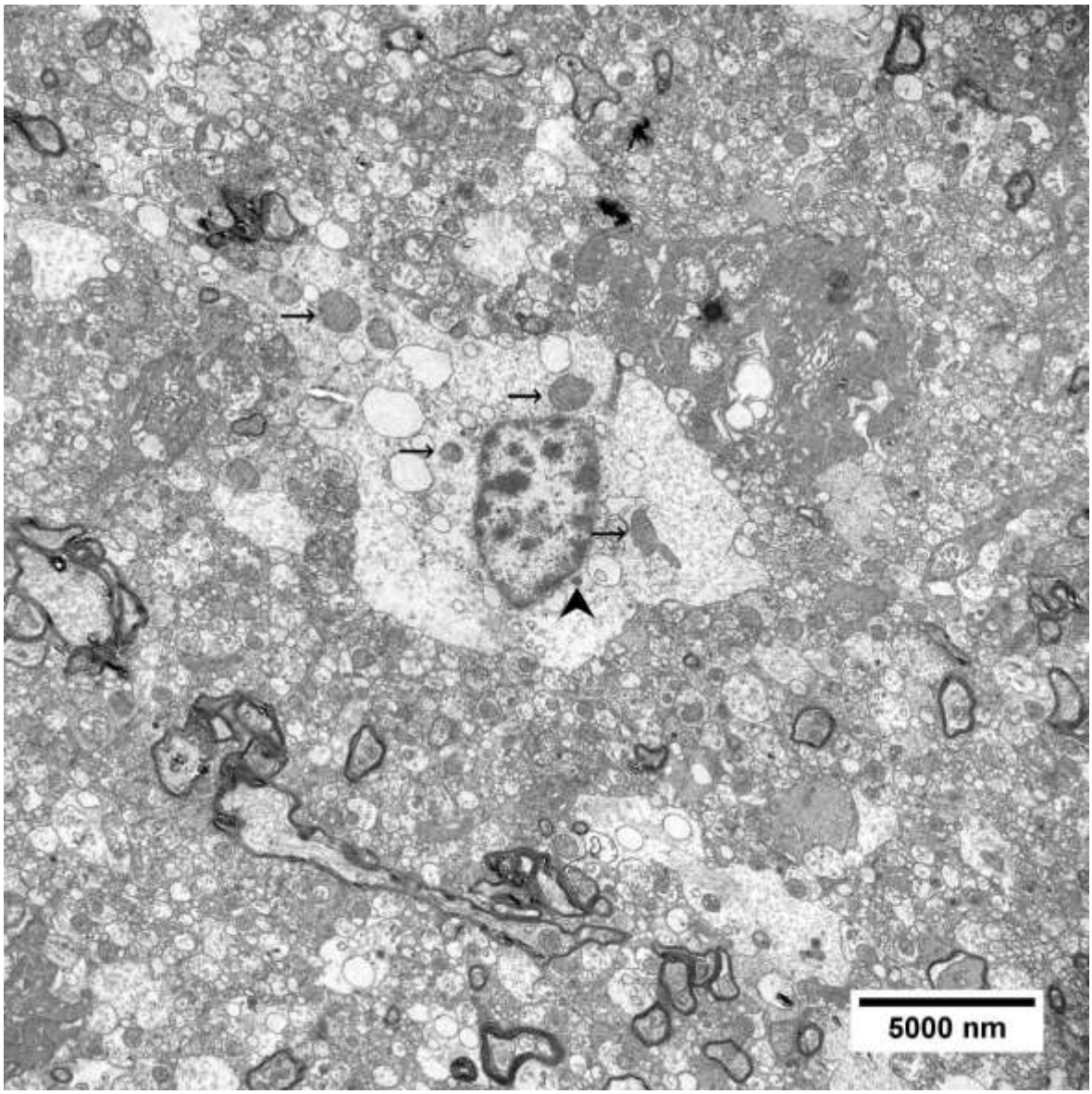

Fig. 24 Neuron at 12 h post-mortem (3000x). Most prominently: the big vacuoles inside the cytoplasm. Also, there are mitochondria (arrows) with nearly no cristae recognizable and a lysosome (arrowhead) at the bottom end of the nucleus.

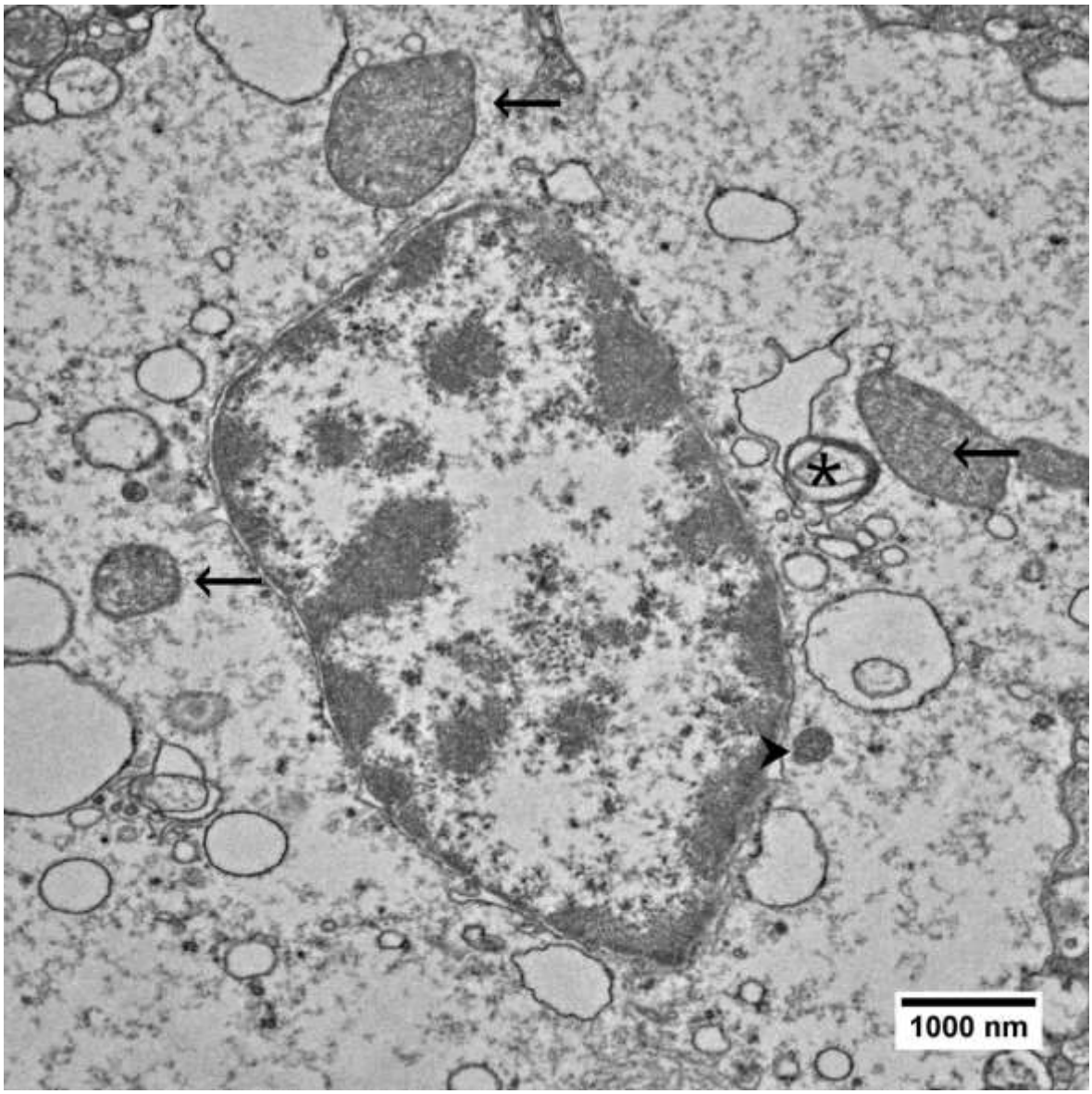

Fig. 25 Neuron at 12 h post-mortem (12000x). Arrows show the mitochondria with nearly no cristae. Arrowhead points to one lysosome and the star shows an autophagosome.

3.2 All cells

The averaged percentages of the occurrence of autolytic changes (with disregard of the maximum cell diameter) in all investigated cells in the PMI are shown in Tab. 4.

Tab. 4 Accordance of all cells (neurons including pyramid cells, astrocytes and oligodendrocytes) with autolytic criteria as followed: condensed chromatin, intracytoplasmic vacuoles, unphysiological ER, structural deviance of mitochondria and occurrence of lysosomes, autophagosomes and autolysosomes in a post-mortem interval of 0 h, 3h, 6 h and 12 h.

	%	%	%	%
Autolytic criteria	**0 h n = 13***	**3 h n = 14**	**6 h n = 12**	**12 h n = 12**
Chromatin	76.9	100.0	100.0	100.0
Vacuoles	0.0	42.9	58.3	66.7
ER	0.0	7.1	0.0	0.0
Mitochondria	0.0	7.1	0.0	25.0

Lysosomes	84.6	85.7	58.3	100.0
Autophagosomes	0.0	28.6	8.3	33.3
Autolysosomes	15.4	21.4	0.0	16.7

*n = number of cells investigated in every point in time

On average, chromatin condensation occurred in 76,92% of all investigated cells at 0 h (Tab. 4). From 3 h to 12 h in the PMI, 100 % of frontal lobe cells showed chromatin condensation.

Intracytoplasmic vacuoles were first seen at 3 h post-mortem, with an average occurrence of 42,86 % at 3 h, 58,33 % at 6 h and 66,67 % at 12 h (Fig. 26).

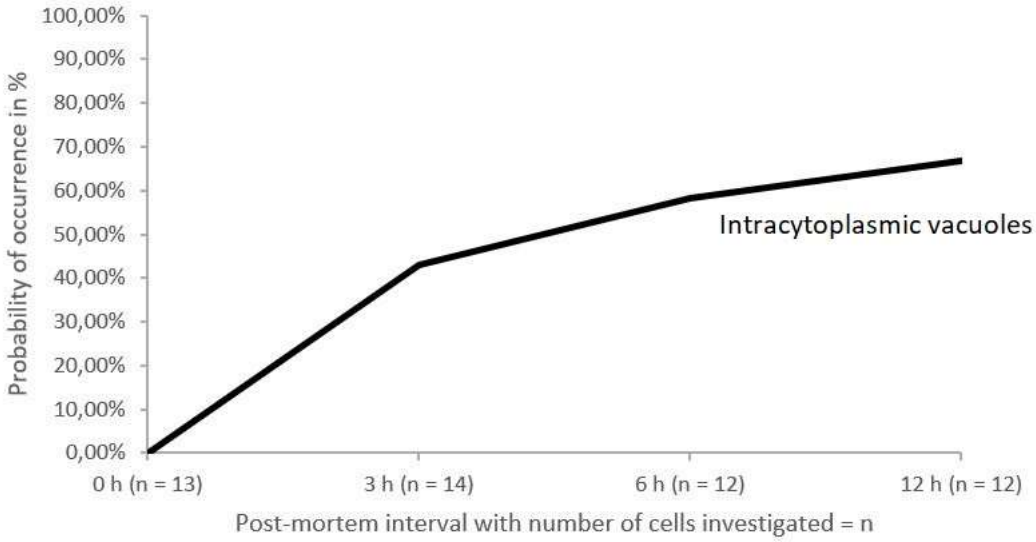

Fig. 26 Probability of occurrence in percent of intracytoplasmic vacuoles in all frontal lobe cells in a post-mortem interval of 0 h, 3 h, 6 h and 12 h.

There were nearly no cells, except for one neuron at 3 h, that met the criteria for autolytic ER (Tab. 4).

The autolytic criteria regarding mitochondria were met with an average occurrence of 7,14 % at 3 h and an occurrence of 25 % at 12 h post-mortem (Fig. 27).

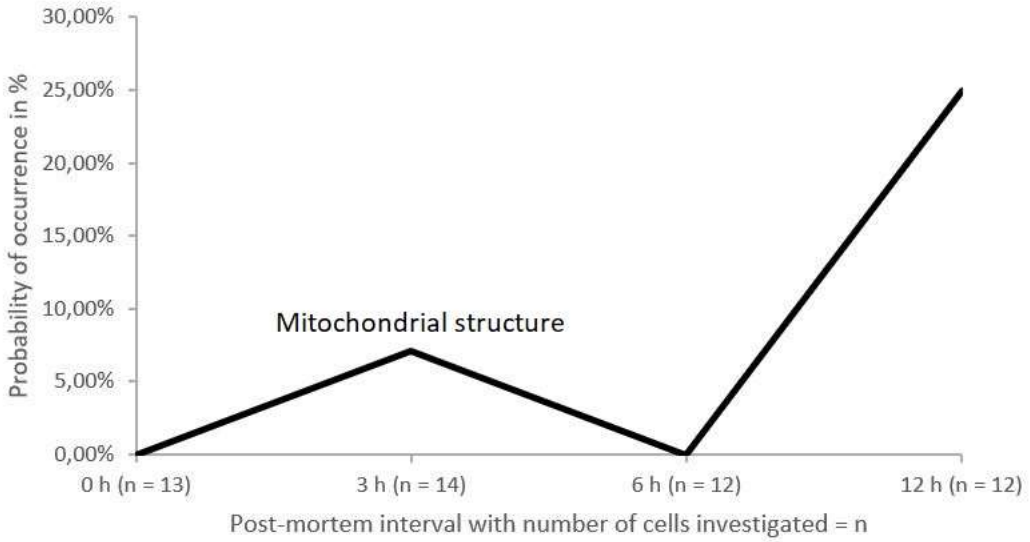

Fig. 27 Probability of occurrence in percent of structural damage of mitochondria in all frontal lobe cells in a post-mortem interval of 0 h, 3 h, 6 h and 12 h.

The occurrence of autolytic changes in lysosomes, autophagosomes and autolysosomes are shown in Fig. 28.

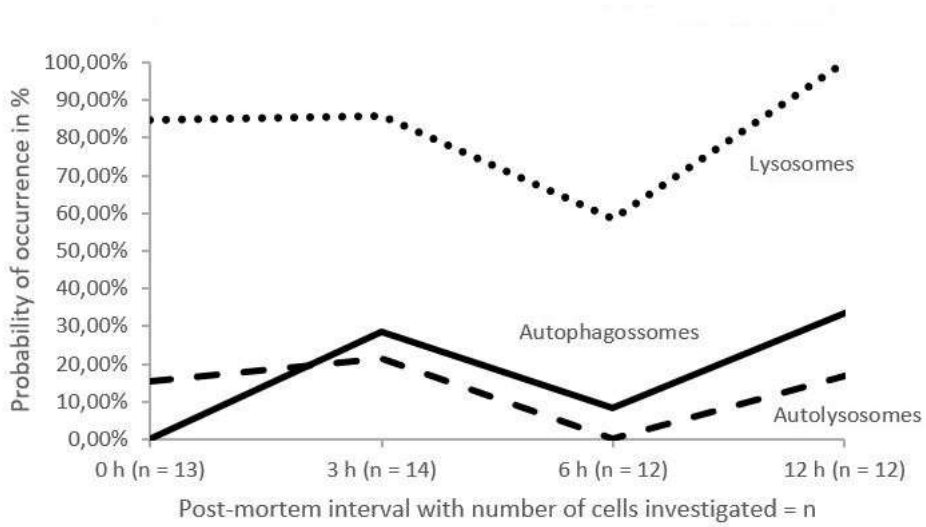

Fig. 28 Probability of occurrence in percent of lysosomes, autophagosomes and autolysosomes in all frontal lobe cells in a post-mortem interval of 0 h, 3 h, 6 h and 12 h.

The maximum cell diameter for each cell type at every point in time in the PMI was averaged and is shown in Tab. 5 as well as in Fig. 29, Fig. 30, Fig. 31 and Fig. 32.

Tab. 5 Increasing and decreasing averaged diameters of cell somata of neurons (with pyramid cells), astrocytes and oligodendrocytes in a post-mortem interval of 0 h, 3h, 6 h and 12 h.

Cell type	0 h		3 h		6 h		12 h	
	µm	n*	µm	n	µm	n	µm	n
Neurons	12.6	2	9.0	1	10.7	4	11.3	2
Pyramid cells	23.2	4	14.7	2	16.6	1	14.2	1
Astrocytes	8.9	4	13.4	6	12.8	3	12.4	5

Oligodendrocytes	9.7	3	10.4	5	10.3	3	10.4	4

*n = number of cells investigated in every point in time

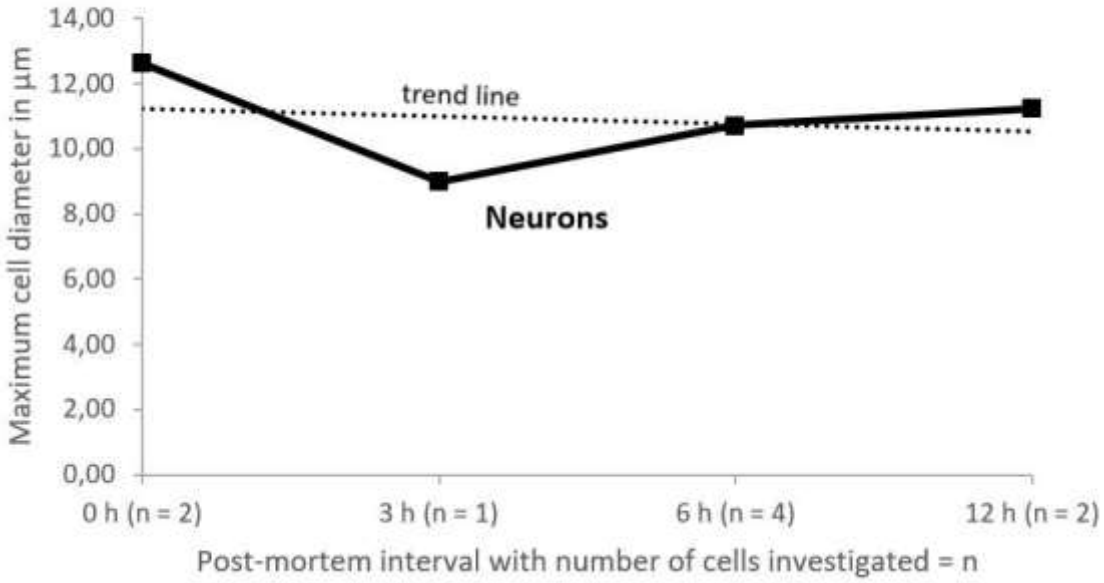

Fig. 29 Averaged maximum cell diameters of all neurons for every point in time in a post-mortem interval of 0 h, 3 h, 6 h and 12 h. The dotted line represents the trend line of the decrease of the cell diameter of neurons.

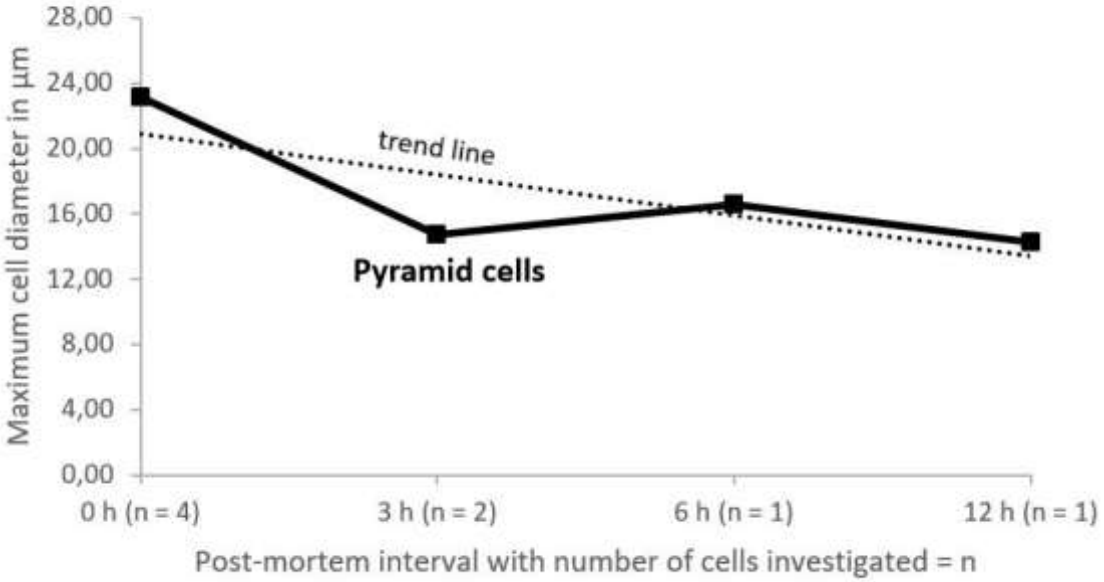

Fig. 30 Averaged maximum cell diameters of all pyramid cells for every point in time in a post-mortem interval of 0 h, 3 h, 6 h and 12 h. The dotted line represents the trend line of the decrease of the cell diameter of pyramid cells.

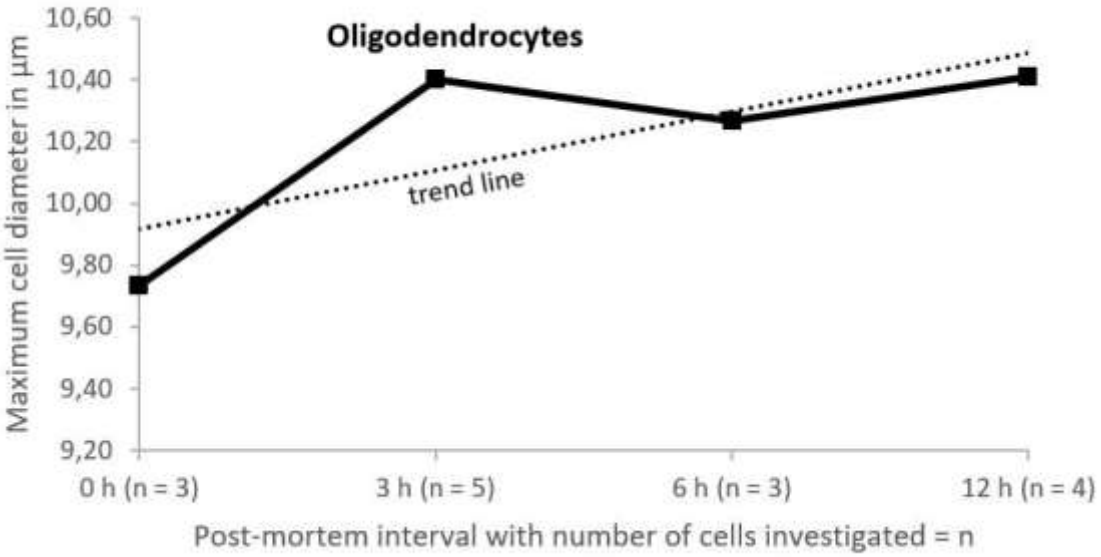

Fig. 31 Averaged maximum cell diameters of all oligodendrocytes for every point in time in a post-mortem interval of 0 h, 3 h, 6 h and 12 h. The dotted line represents the trend line of the increase of the cell diameter of oligodendrocytes.

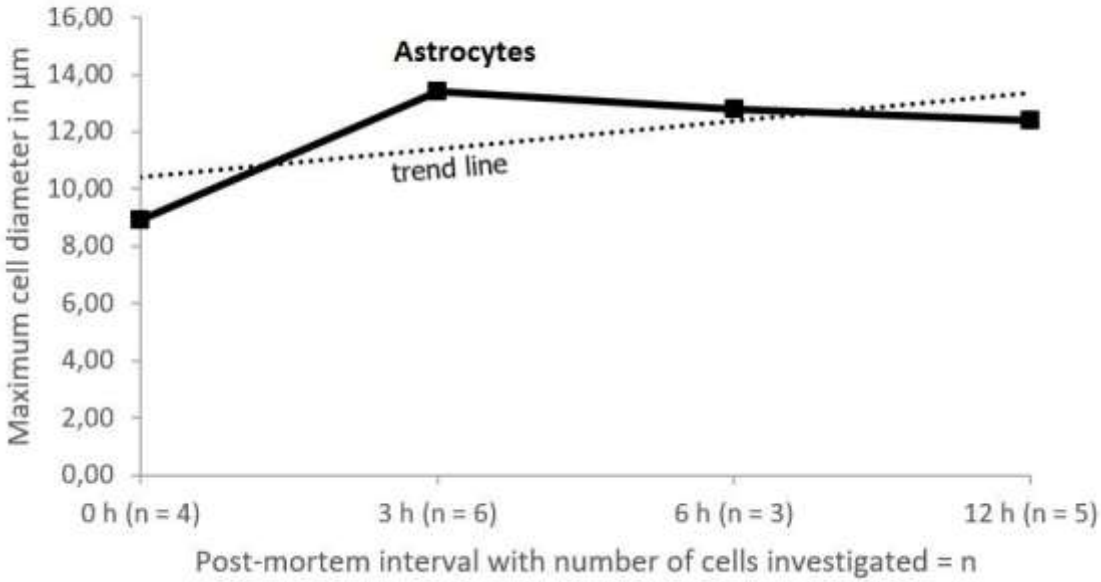

Fig. 32 Averaged maximum cell diameters of all astrocytes for every point in time in a post-mortem interval of 0 h, 3 h, 6 h and 12 h. The dotted line represents the trend line of the increase of the cell diameter of oligodendrocytes.

After 12 h the diameter of neuronal cells tended to decrease (neurons: 12,61 µm to 11,25 µm; pyramid cells: 23,15 µm to 14,24 µm) while glial cells rather gained in diameter (astrocytes: 8,9 µm to 12,4 µm; oligodendrocytes: 9,73 µm to 10,41 µm).

3.3 Grey matter vs. white matter

We found differences between grey and white matter cells in the autolytic criteria regarding the intracytoplasmic vacuoles and the autolytic organelles lysosomes, autophagosomes and autolysosomes (Fig. 33, Fig. 34, Fig. 35 and Fig. 36).

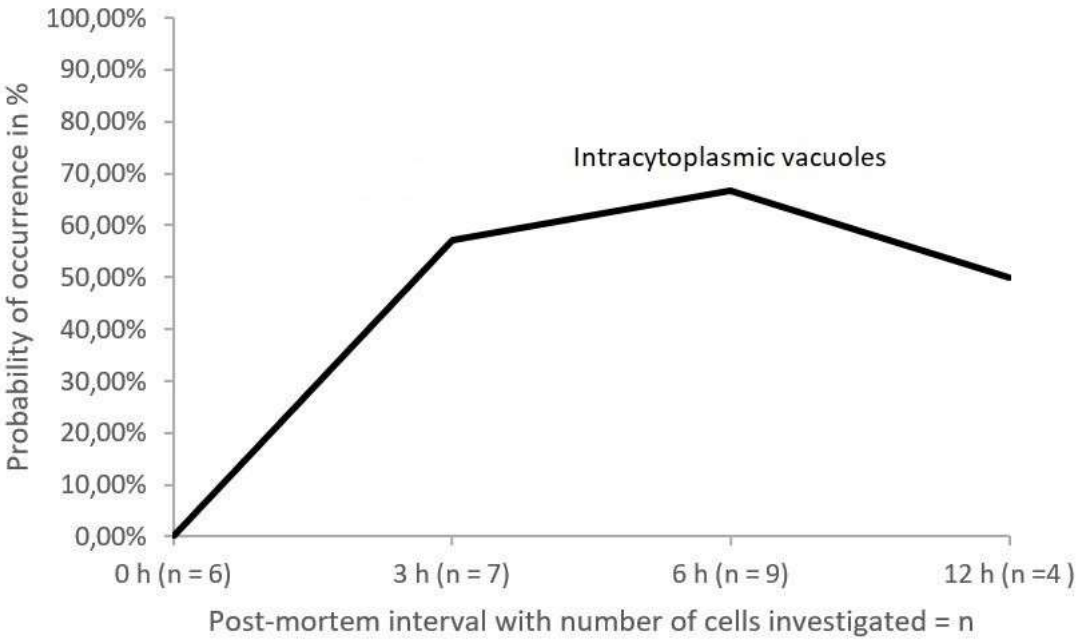

Fig. 33 Probability of occurrence in percent of intracytoplasmic vacuoles in cells of the grey matter of the frontal lobe in a post-mortem interval of 0 h, 3 h, 6 h and 12 h.

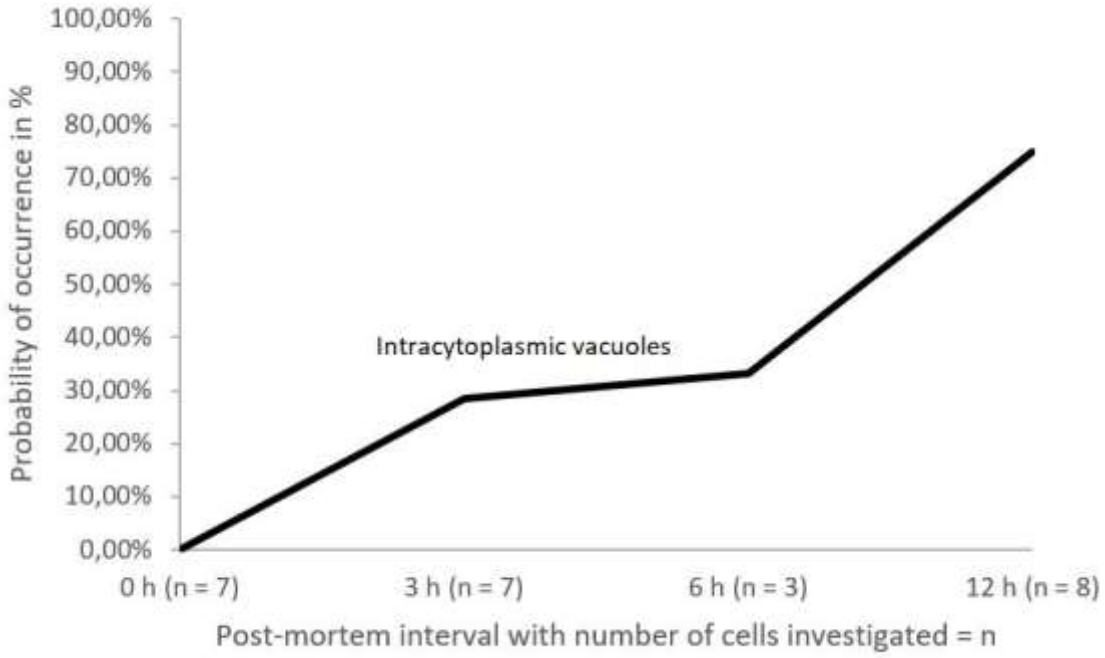

Fig. 34 Probability of occurrence in percent of intracytoplasmic vacuoles in cells of the white matter of the frontal lobe in a post-mortem interval of 0 h, 3 h, 6 h and 12 h.

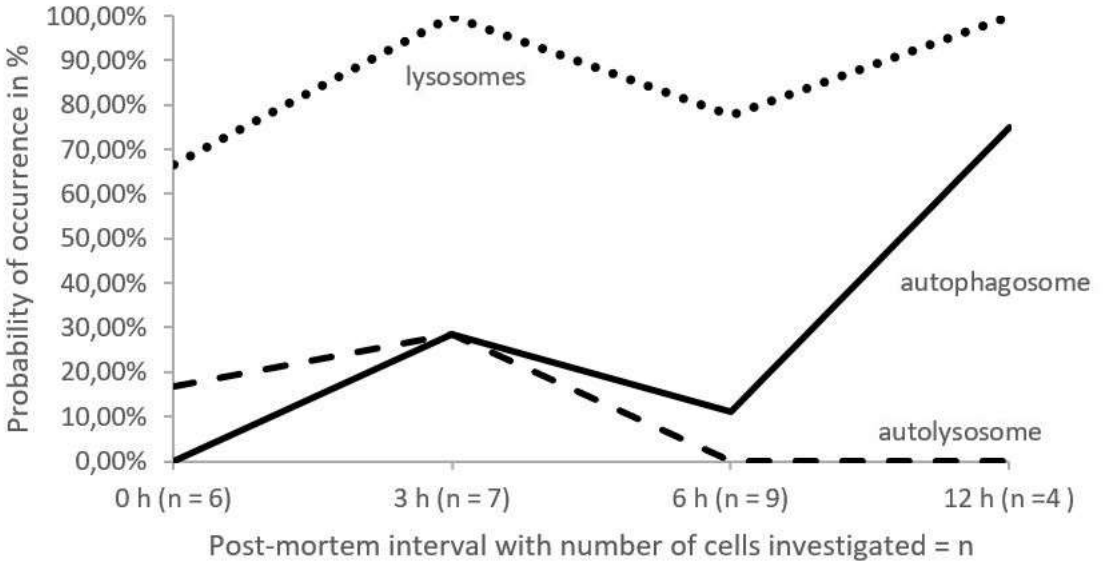

Fig. 35 Probability of occurrence in percent of lysosomes, autophagosomes and autolysosome in cells of the grey matter of the frontal lobe in a post-mortem interval of 0 h, 3 h, 6 h and 12 h.

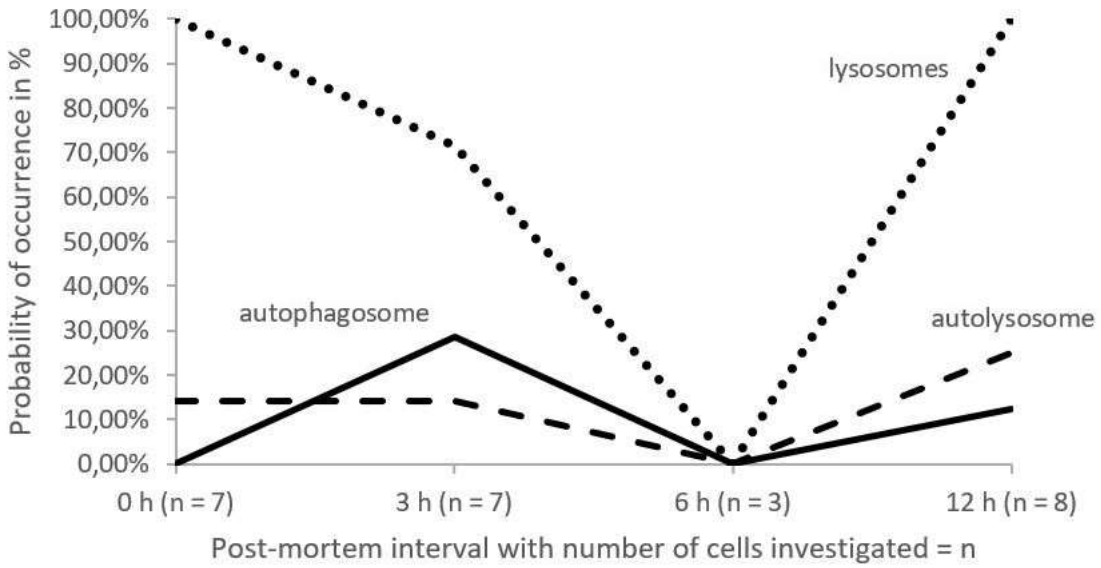

Fig. 36 Probability of occurrence in percent of lysosomes, autophagosomes and autolysosome in cells of the white matter of the frontal lobe in a post-mortem interval of 0 h, 3 h, 6 h and 12 h.

While in the grey matter the occurrence of intracytoplasmic vacuoles tended to increase to 66,67 % at 6 h and then decreased at 12 h, the occurrence of vacuoles in white matter cells increased continuously until 12 h (Fig. 33 and Fig. 34).

Lysosomes, autophagosomes and autolysosomes also showed differences in their probability to occur at 6 hours. On the one hand, there was neither one of said organelles visible in the white matter (Fig. 36). On the other hand, lysosomes appeared in 77,78 % of grey matter cells at 6 hours and autophagosomes in 11,11 % (Fig. 32). Autolysosomes were neither found in grey, nor white matter cells at 6 h post-mortem.
Also, the occurrence of autophagosomes in grey matter cells at 12 h was higher than in white matter cells (75,00 % vs. 12,50 %).

3.4 Neurons vs. glia cells

There were also slight differences between neurons (including pyramid cells) and glial cells (astrocytes and oligodendrocytes) regarding post-mortem autolytic changes, especially regarding the occurrence of intracytoplasmic vacuoles, lysosomes, autophagosomes and autolysosomes (Fig. 37, Fig. 38 and Fig. 39, Fig. 40).

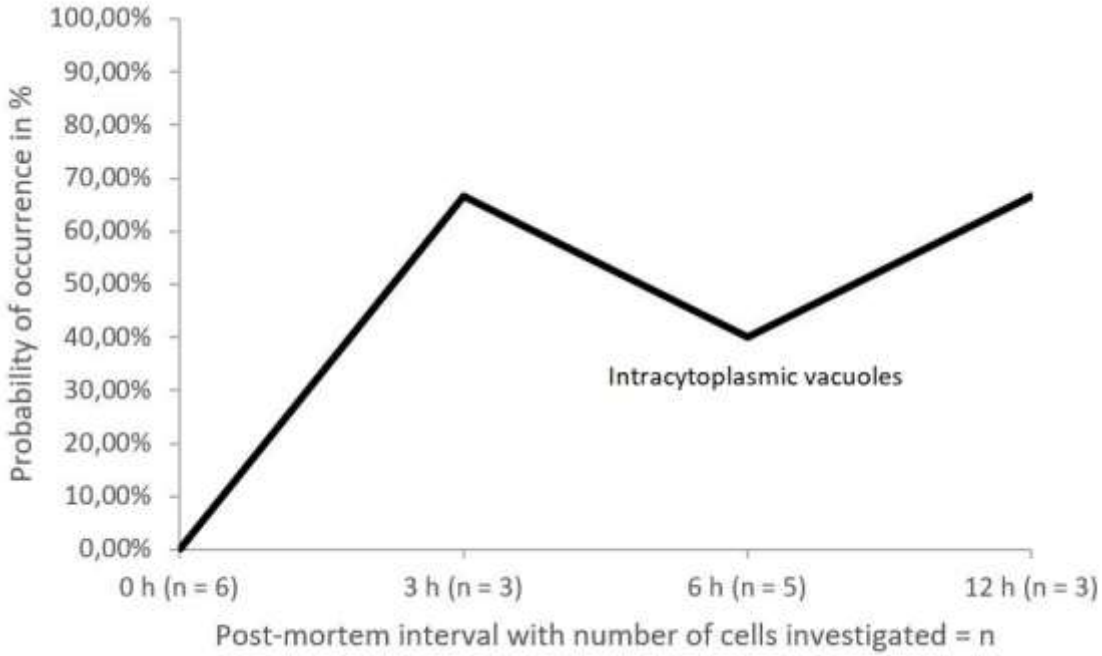

Fig. 37 Probability of occurrence in percent of intracytoplasmic vacuoles in neurons (including pyramid cells) of the frontal lobe in a post-mortem interval of 0 h, 3 h, 6 h and 12 h.

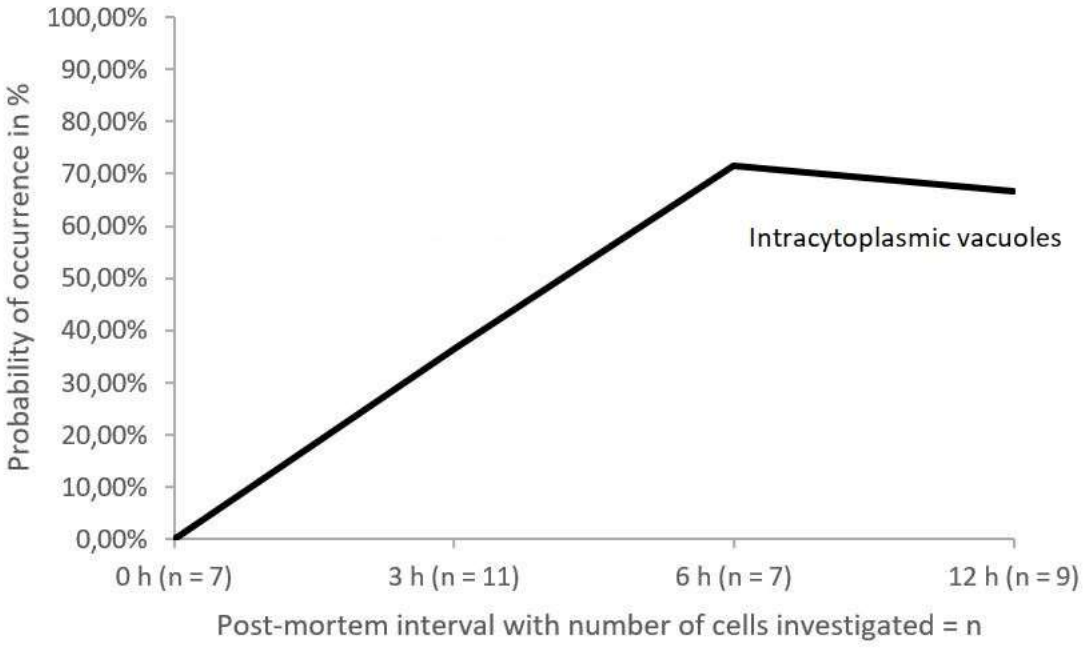

Fig. 38 Probability of occurrence in percent of intracytoplasmic vacuoles in glial cells (astrocytes and oligodendrocytes) of the frontal lobe in a post-mortem interval of 0 h, 3 h, 6 h and 12 h.

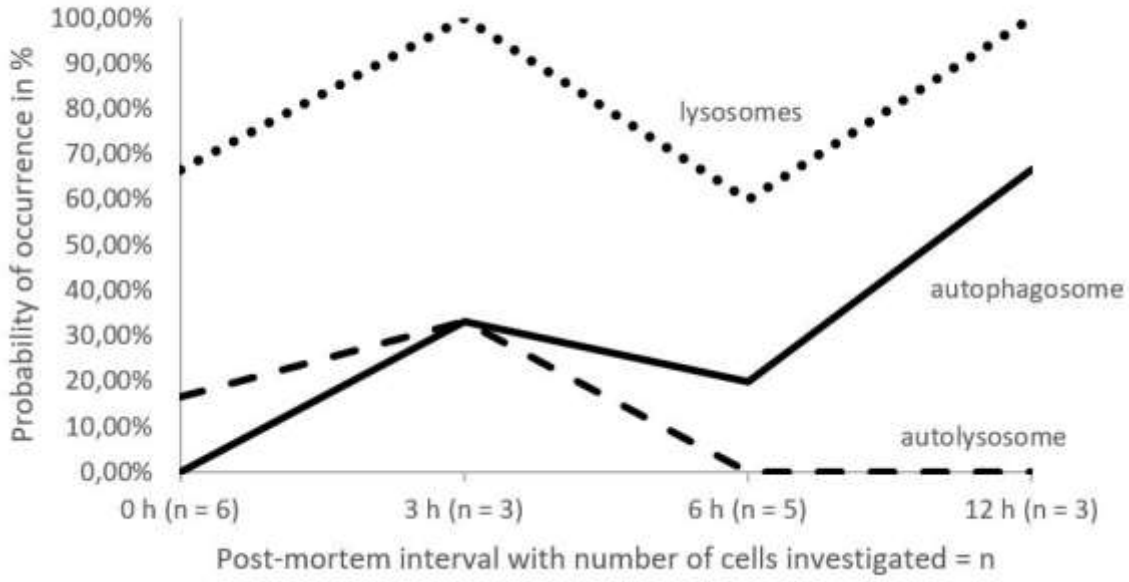

Fig. 39 Probability of occurrence in percent of lysosomes, autophagosomes and autolysosome in neurons (including pyramid cells) of the frontal lobe in a post-mortem interval of 0 h, 3 h, 6 h and 12 h.

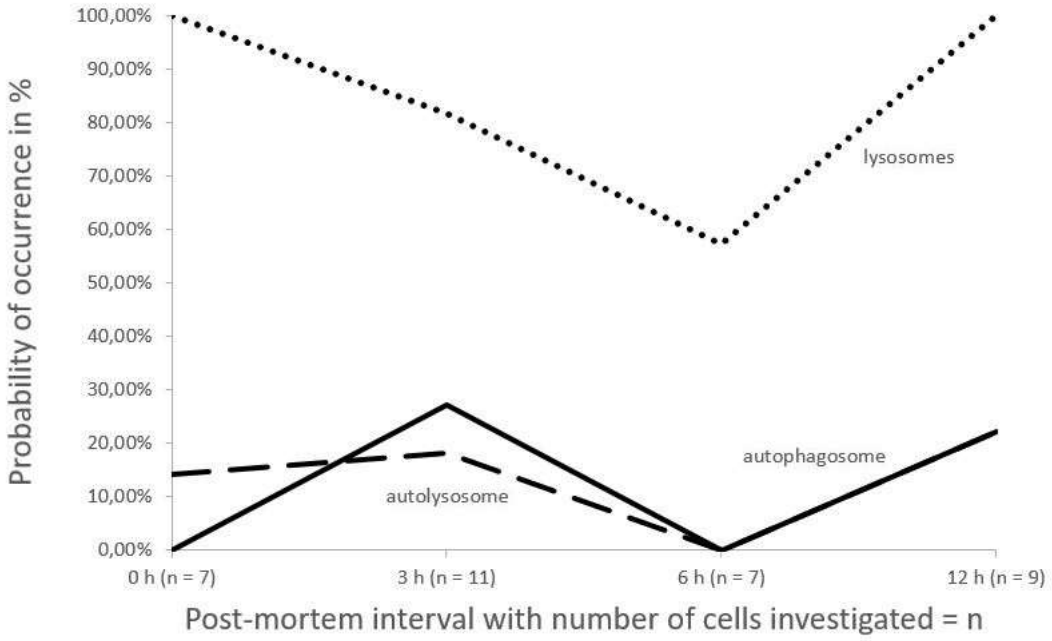

Fig. 40 Probability of occurrence in percent of lysosomes, autophagosomes and autolysosome in glial cells (astrocytes and oligodendrocytes) of the frontal lobe in a post-mortem interval of 0 h, 3 h, 6 h and 12 h.

In neurons, there is an occurrence of 66,67 % of intracytoplasmic vacuoles at 3 h, while in glial cells only 36,36 % show these changes (Fig. 37 and Fig. 38). Furthermore, the probability of vacuoles appearing tended to decrease from 3 to 6 h in neurons while steadily increasing in glial cells in the same time span.

The most profound difference between neurons and glial cells was the occurrence of autophagosomes at 12 h post-mortem (66,67 % in neurons vs. 22,22 % in glial cells; Fig. 39 and Fig. 40).

4 Discussion

4.1 Main message

First and foremost, our work shows that in a post-mortem interval (PMI) of 12 h autolysis is apparent in frontal lobe cells of *Sus scrofa*. We used such a timespan because if we had fixed all cells immediately after death, we could not see any autolytic changes – those appear after a certain time post-mortem. The increase of chromatin condensation, cell volume changes throughout the PMI, intracytoplasmic vacuolization and the occurrence of lysosomes during the period of 12 hours post-mortem confirm our hypothesis of the existence of autolytic processes in pig neurons, astrocytes and oligodendrocytes.

4.2 Critical assessment

The biggest limitation of this work is that we investigated the ultrastructural changes of three-dimensional objects (cells) with two-dimensional images. Therefore, we were not able to elucidate the morphology of whole cells within the frontal lobe, neither in glial cells nor in neurons and could possibly have missed ultrastructural changes in other areas of the cell.

The second biggest limitation of our study is that we did not control the intrinsic or extrinsic factors influencing the speed of post-mortem changes such as humidity of the environment, physical state of the pig or the overall health of the animal. The storage temperature was normal room-temperature, which is subject to fluctuations.

Besides, we only had one specimen of a species of which we only investigated a small number of cells at each point in time (sometimes only one cell body from a cell type at a specific hour; e.g. pyramid cells at 6 h).

Furthermore, the autolytic criteria we used are not standardized and there is neither a consensus for these criteria as such, nor is there any publication describing the exact sequence of events during post-mortem autolysis. One reason for this is that the use of the term “autolysis” within the scientific community is unspecific.

Also, for the criterion of the maximum diameter of a cell soma one must initially find a cell body with an intact nucleus. Otherwise it would have been impossible to investigate any cell body at all. The problem with this procedure here is, that we automatically discharged the possibility of finding any karyolitic cells, which is a strong indicator for autolysis (George et al., 2016, p. 4).

Moreover, some of the criteria are only used inside of the cell boundaries of a single cell body on the one hand (e.g. unphysiological ER) while other criteria are used for a single

image by investigating multiple cells on the other hand (e.g. mitochondrial structure). This procedure could distort the occurrence of those autolytic criteria which refer to multiple cells in an image.

Additionally, the anatomy of the pig telencephalon is not fully understood. Some authors have conflicting views regarding the location of the frontal and parietal lobe. Therefore, there is a small chance, that the samples may have been taken from the area that some authors call parietal lobe (Lind et al., 2007, p. 733).

Finally, the time needed for the first extirpation of brain matter was round about one hour, which means, that the actual post-mortem interval is shifted by adding one hour to every point in time.

4.3 Comparison with other studies

To construct the autolytic criteria used in our study, we worked through several papers on the subject. These papers, which investigate post-mortem changes in the brain of mammals and rodents, are highly ambivalent in their study design. Because our animal underwent a global cerebral ischaemia as a catastrophic brain injury (CBI), we divided all studies used for creating our autolytic criteria into global and local ischaemia groups (Tab. 6).

Tab. 6 Authors investigating post-mortem changes or autolysis in the brain of mammals and rodents. The table is divided into authors that studied global brain ischaemia and authors who worked on focal ischaemia or other forms of brain damage. Also, the study animals used in their papers are listed on the right-hand side.

Authors	Global ischaemia	Focal ischaemia and others	Animal models
(Suzuki, 2013)	x		not clear
(Sheleg et al., 2008)	x		Wistar rats
(Kalimo et al., 1977)	x		Cats
(Hirsch and Müller, 1962)	x		Rabbit
(Paternoster et al., 2019)	x		Human
(Fountoulakis et al., 2001)	x		Rat
(Scheuerle et al., 1993)	x		Mouse
(Kraupp et al., 1995)	x		Wistar rat
(Gonzalez-Riano et al., 2017)	x		Mouse
(Xu and Zhang, 2011)		Ischaemia/hypoxia	Mouse
(Panickar and Norenberg, 2005)		Ischaemia	Human
(Liu and Levine, 2015)		Not clear	Human
(Garcia et al., 1978)		Ischeamia	Cat and monkey
(Dettmeyer, 2011)		Not clear	Human
(Matyash and Kettenmann, 2010)		Not clear	Human
(Stinnett et al., 2017)		Not clear	Pig
(Pannese and Ferrannini, 1967)		Perfusation fixation/ Not clear	Cat & guinea pig
(MacKenzie, 2014)		Not clear	Human

As a result, we placed greater emphasis on global ischaemia studies that investigated mammals like humans, monkeys, or cats when deciding which criteria we chose for autolysis.

Throughout the PMI, we found chromatin condensation in 48 of 51 cases. All cells that showed no chromatin condensation were found at 0 h post-mortem. Therefore, beginning from 3 h post-mortem, all the investigated cells (regardless of the cell type) showed chromatin condensation. This result is coherent with the results of Kalimo et al., who describe chromatin clumping occurring as soon as 10 min after death in cat brains (Kalimo et al., 1977, p. 209). Also, according to Dettmeyer et al., chromatin agglutination in nerve cells takes place as soon as a few minutes after ischemic or hypoxic brain damage (Dettmeyer, 2011, p. 420). Furthermore, chromatin clumping is seen at 6 h post-mortem as stated by Garcia et al. and Xu et al. (Garcia et al., 1978, p. 86; Xu and Zhang, 2011, p. 1092). We therefore think that chromatin condensation is a strong indicator for post-mortem autolysis.

Moreover, our results show that the cell bodies of neurons tend to shrink after a PMI of 12 hours, whereas the somata of astrocytes and oligodendrocytes (and therefore glial cells) tend to increase in volume. These different cellular volume alterations exactly match those described by Garcia et al. According to their study, during ischaemia, neurons shrink, while oligodendrocytes and astrocytes tend to swell (Garcia et al., 1978, p. 88). Kalimo et al., Panickar et al. and Suzuki also describe post-mortem or ischemic astrocyte swelling (Kalimo et al., 1977, p. 209; Panickar and Norenberg, 2005, p. 289; Suzuki, 2013, p. 46). Moreover, neurons of mice also shrink after 24 h in ischemic-hypoxic brain injury as stated by Xu and Zhang (Xu and Zhang, 2011, p. 1092). These studies in addition to our own results show that volume changes of the different types of cells in the pig brain are also an adequate marker for autolysis.

In the results section of our study, we describe intracytoplasmic vacuolization in 21 of 51 cells. Nevertheless, the trend of the occurrence of intracytoplasmic vacuolization shows a continuous increase from 0 h (0 of 13 cells) to 12 h (8 of 12 cells). Quite a few authors also describe intracytoplasmic vacuolization with regards to post-mortem autolysis. While Xu et al. state intense vacuolization of mouse neurons paired with the appearance of numerous autophagosomes after 24 h in ischaemia, Garcia et al. found many big vacuoles in neurons

after regional brain ischaemia (Garcia et al., 1978, p. 88; Xu and Zhang, 2011, p. 1092). Suzuki also found microvacuoles in neurons that underwent focal ischaemia (Suzuki, 2013, p. 25) and intracytoplasmic vacuoles in astrocytes that formed after global ischaemia (Suzuki, 2013, p. 48). In accordance with the results of these authors, our findings regarding intracytoplasmic vacuolization as a criterion for autolytic processes can be regarded as coherent with post-mortem autolysis in pig frontal lobe cells.

We found lysosomes in 42 of 51 investigated cells in our study. In addition to the high incidence of lysosomes in all the PMIs examined, there was also an increasing trend of the occurrence of lysosomes beginning at 0 h (11 out 13 cells) to 12 h (12 out of 12 cells). Two papers also support the occurrence of lysosomes in post-mortem autolysis. Sheleg et al. show an occurrence of lysosomes as early as 6 h post-mortem with a slightly swollen appearance (Sheleg et al., 2008, pp. 292–293), while Xu et al. describe a rise in the count of lysosomes from 3 h to 12 h in the PMI (Xu and Zhang, 2011, p. 1092). Again, because our experimental results are in accordance with the findings of other authors investigating post-mortem changes, this study confirms that the appearance and rise in count of lysosomes are strong indicators for post-mortem autolysis.

Out of 51 cells, we only found 9 cells with autophagosomes and 7 cells with autolysosomes in all the PMIs. Also, there was no clear trend in the occurrence of these organelles in post-mortem brain cells of our pig. We investigated the occurrence of autophagosomes and autolysosomes in global brain ischaemia, because we hypothesised that these organelles have a minor role in post-mortem autolysis through global brain ischaemia (Fricker et al., 2018, p. 828). They are rather important in type II cell death, or autophagy (Fricker et al., 2018, p. 828; Galluzzi et al., 2018, p. 487). The low and inconsistent count of autophagosomes and autolysosomes in our results can therefore be explained as followed: because autophagic cell death mechanisms are active processes which require ATP to function, the shortage of said molecule in our study animal can supress the process of this cell death type (Fricker et al., 2018, pp. 827–828). Since these two organelles play a dominant role in autophagy (Fricker et al., 2018, p. 828), the occurrence of them is decreased. Comparing this result with the result of the occurrence of lysosomes in the frontal lobe of our study animal, we conclude that our findings are coherent with the expected outcome of the ultrastructural analysis of the investigated cells.

Only one out of 51 cells in the entire PMI matched our criteria for unphysiological ER. Because the morphology of nearly all endoplasmic reticula investigated showed a more circular than elongated structure as a sign of swelling, we had to expand our autolytic criteria with another sign of ER-alteration. Because Kalimo et al. showed that ribosomes detach from rER after 30 min post-mortem (Kalimo et al., 1977, p. 209) and Suzuki describes an increase of free ribosomes in the cytoplasm due to the detachment of ribosomes from the ER after 1 h (Suzuki, 2013, p. 48), we concluded that we have to add the transition from rough endoplasmic reticula with ribosomes to rough endoplasmic reticula without ribosomes to our autolytic criteria. Additionally, Xu et al. describe fragmented ER after 6 h post-mortem in neurons with regards to autolysis (Xu and Zhang, 2011, p. 1092), while Panickar et al. show an increase of the count of ER in astrocytes after ischaemia (Panickar and Norenberg, 2005, p. 290). For reasons of practicality, we disregarded the findings of Xu and Panickar as another part of our criteria for unphysiological ER. Therefore, our criteria were as follows: The ER had to be (a) circular and not elongated in its structure and (b) there should only be rough ER without ribosomes apparent, especially not near the nucleus, as a sign of the detachment of ribosomes from the ER. In spite of the fact that we found many circular and therefore swollen endoplasmic reticula, there was nearly no cell body with the detachment of all ribosomes from rough ER. Although we do not fully understand, why the incidence of unphysiological ER is so low, we hypothesize, that it is likely that rather only a few rER transition to rER without ribosomes, than every single cistern of rER losing its ribosomes. Thus, we state that this criterion is a rather weak indicator for post-mortem autolysis.

Finally, we only found 4 cells out of 51 which matched our autolytic criteria for mitochondria.

Kalimo et al. report rounded mitochondria with a less dense matrix after 30 minutes as well as a slight swelling and occasional floccular densities inside the matrix (Kalimo et al., 1977, p. 209). Suzuki shows mitochondrial swelling in neurons after 1 h (Suzuki, 2013, p. 49) as well as Sheleg et al., only after 3 h (Sheleg et al., 2008, p. 293). Also, Garcia et al. showed a swelling in astrocyte mitochondria as well as the appearance of matrical densities after 7 h post-mortem (Garcia et al., 1978, p. 88). Furthermore Panickar et al. investigated that after ischaemia, the overall count of mitochondria in astrocytes rises (Panickar and Norenberg, 2005, p. 290). The low incidence of these criteria in our results could be due to the fact that we investigated every mitochondrion in every image instead of only the

mitochondria of a single cell. The reason we did this was that we did not always find mitochondria in every cell. Since there are manifold ultrastructural changes to mitochondria as stated above, we chose a rather radical approach and stated autolytic criteria that were only met when all the mitochondria in the image showed either damaged cristae or damaged mitochondrial membranes while possibly having a swollen appearance. Perhaps, a measure of the average diameter of the transversely cut mitochondria throughout the PMI with an investigation of the trend of the averaged diameter as a sign of swelling or shrinking, could be a better criterion for the ultrastructural changes of mitochondria in post-mortem autolysis. We therefore conclude that this criterion is a rather weak indicator of post-mortem autolysis in pig brain cells.

4.4 Conclusions

Despite many limitations, this descriptive work confirms several post-mortem autolytic ultrastructural changes in neural and glial cells described in other study animals. It also shows that the exact criteria for post-mortem autolytic cell death (or post-mortem autolysis) on an ultrastructural level are not yet fully understood.

Therefore, to get a better understanding of post-mortem changes of brain cells, clear definitions of the terms *autolysis* and *post-mortem autolysis*, a standardization of criteria for these terms and a strict control of intrinsic and extrinsic (environmental) experimental factors through future research are inevitable.

5 Literature

Dettmeyer, R.B., 2011. Forensic Histopathology: Fundamentals and Perspectives, 1st ed. Springer, Heidelberg.

Donaldson, A.E., Lamont, I.L., 2013. Biochemistry Changes That Occur after Death: Potential Markers for Determining Post-Mortem Interval. PLoS ONE 8, e82011. https://doi.org/10.1371/journal.pone.0082011

Fountoulakis, M., Hardmeier, R., Höger, H., Lubec, G., 2001. Postmortem Changes in the Level of Brain Proteins. Exp. Neurol. 167, 86–94. https://doi.org/10.1006/exnr.2000.7529

Fricker, M., Tolkovsky, A.M., Borutaite, V., Coleman, M., Brown, G.C., 2018. Neuronal Cell Death. Physiol Rev 98, 68.

Galluzzi, L., Vitale, I., Aaronson, S.A., Abrams, J.M., Adam, D., Agostinis, P., Alnemri, E.S., Altucci, L., Amelio, I., Andrews, D.W., Annicchiarico-Petruzzelli, M., Antonov, A.V., Arama, E., Baehrecke, E.H., Barlev, N.A., Bazan, N.G., Bernassola, F., Bertrand, M.J.M., Bianchi, K., Blagosklonny, M.V., Blomgren, K., Borner, C., Boya, P., Brenner, C., Campanella, M., Candi, E., Carmona-Gutierrez, D., Cecconi, F., Chan, F.K.-M., Chandel, N.S., Cheng, E.H., Chipuk, J.E., Cidlowski, J.A., Ciechanover, A., Cohen, G.M., Conrad, M., Cubillos-Ruiz, J.R., Czabotar, P.E., D'Angiolella, V., Dawson, T.M., Dawson, V.L., De Laurenzi, V., De Maria, R., Debatin, K.-M., DeBerardinis, R.J., Deshmukh, M., Di Daniele, N., Di Virgilio, F., Dixit, V.M., Dixon, S.J., Duckett, C.S., Dynlacht, B.D., El-Deiry, W.S., Elrod, J.W., Fimia, G.M., Fulda, S., García-Sáez, A.J., Garg, A.D., Garrido, C., Gavathiotis, E., Golstein, P., Gottlieb, E., Green, D.R., Greene, L.A., Gronemeyer, H., Gross, A., Hajnoczky, G., Hardwick, J.M., Harris, I.S., Hengartner, M.O., Hetz, C., Ichijo, H., Jäättelä, M., Joseph, B., Jost, P.J., Juin, P.P., Kaiser, W.J., Karin, M., Kaufmann, T., Kepp, O., Kimchi, A., Kitsis, R.N., Klionsky, D.J., Knight, R.A., Kumar, S., Lee, S.W., Lemasters, J.J., Levine, B., Linkermann, A., Lipton, S.A., Lockshin, R.A., López-Otín, C., Lowe, S.W., Luedde, T., Lugli, E., MacFarlane, M., Madeo, F., Malewicz, M., Malorni, W., Manic, G., Marine, J.-C., Martin, S.J., Martinou, J.-C., Medema, J.P., Mehlen, P., Meier, P., Melino, S., Miao, E.A., Molkentin, J.D., Moll, U.M., Muñoz-Pinedo, C., Nagata, S., Nuñez, G., Oberst, A., Oren, M., Overholtzer, M., Pagano, M., Panaretakis, T., Pasparakis, M., Penninger, J.M., Pereira, D.M., Pervaiz, S., Peter, M.E., Piacentini, M., Pinton, P., Prehn, J.H.M., Puthalakath, H., Rabinovich, G.A., Rehm, M., Rizzuto, R., Rodrigues, C.M.P., Rubinsztein, D.C., Rudel, T., Ryan, K.M., Sayan, E., Scorrano, L., Shao, F., Shi, Y., Silke, J., Simon, H.-U., Sistigu, A., Stockwell, B.R., Strasser, A., Szabadkai, G., Tait, S.W.G., Tang, D., Tavernarakis, N., Thorburn, A., Tsujimoto, Y., Turk, B., Vanden Berghe, T., Vandenabeele, P., Vander Heiden, M.G., Villunger, A., Virgin, H.W., Vousden, K.H., Vucic, D., Wagner, E.F., Walczak, H., Wallach, D., Wang, Y., Wells, J.A., Wood, W., Yuan, J., Zakeri, Z., Zhivotovsky, B., Zitvogel, L., Melino, G., Kroemer, G., 2018. Molecular mechanisms of cell death: recommendations of the Nomenclature Committee on Cell Death 2018. Cell Death Differ. 25, 486–541. https://doi.org/10.1038/s41418-017-0012-4

Garcia, J.H., Lossinsky, A.S., Kauffman, F.C., Conger, K.A., 1978. Neuronal ischemic injury: Light microscopy, ultrastructure and biochemistry. Acta Neuropathol. (Berl.) 43, 85–95. https://doi.org/10.1007/BF00685002

George, J., Van Wettere, A.J., Michaels, B.B., Crain, D., Lewbart, G.A., 2016. Histopathologic evaluation of postmortem autolytic changes in bluegill (*Lepomis macrohirus*) and crappie (*Pomoxis anularis*) at varied time intervals and storage temperatures. PeerJ 4, e1943. https://doi.org/10.7717/peerj.1943

Gonzalez-Riano, C., Tapia-González, S., García, A., Muñoz, A., DeFelipe, J., Barbas, C., 2017. Metabolomics and neuroanatomical evaluation of post-mortem changes in the hippocampus. Brain Struct. Funct. 222, 2831–2853. https://doi.org/10.1007/s00429-017-1375-5

Harle, L., 2019. Forensic pathology (general): Postmortem changes [WWW Document]. PathologyOutlines.com. URL https://www.pathologyoutlines.com/topic/forensicspostmortem.html (accessed 10.3.19).

Hirsch, H., Müller, H.A., 1962. Funktionelle und histologische Veränderungen des Kaninchengehirns nach kompletter Ischämie. Pflüg. Arch. Für Gesamte Physiol. Menschen Tiere 275, 277–291. https://doi.org/10.1007/BF00362190

Kalimo, H., Garcia, J.H., Kamijyo, Y., Tanaka, J., Trump, B.F., 1977. The Ultrastructure of "Brain Death" 14.

Kraupp, B.G., Ruttkay-Nedecky, B., Koudelka, H., Bukowska, K., Bursch, W., Schulte-Hermann, R., 1995. In situ detection of fragmented dna (tunel assay) fails to discriminate among apoptosis, necrosis, and autolytic cell death: A cautionary note. Hepatology 21, 1465–1468. https://doi.org/10.1002/hep.1840210534

Kuehnel, W., Kuehnel, W., 2003. Color Atlas of Cytology, Histology, and Microscopic Anatomy. Georg Thieme Verlag. https://doi.org/10.1055/b-005-148882

Lind, N.M., Moustgaard, A., Jelsing, J., Vajta, G., Cumming, P., Hansen, A.K., 2007. The use of pigs in neuroscience: Modeling brain disorders. Neurosci. Biobehav. Rev. 31, 728–751. https://doi.org/10.1016/j.neubiorev.2007.02.003

Liu, Y., Levine, B., 2015. Autosis and autophagic cell death: the dark side of autophagy. Cell Death Differ. 22, 367–376. https://doi.org/10.1038/cdd.2014.143

MacKenzie, J.M., 2014. Examining the Decomposed Brain: Am. J. Forensic Med. Pathol. 35, 265–270. https://doi.org/10.1097/PAF.0000000000000111

Martínez, P.N., Menéndez, S.T., Villaronga, M. de los Á., Ubelaker, D.H., García-Pedrero, J.M., C. Zapico, S., 2019. "The big sleep: Elucidating the sequence of events in the first hours of death to determine the postmortem interval." Sci. Justice 59, 418–424. https://doi.org/10.1016/j.scijus.2019.03.001

Matyash, V., Kettenmann, H., 2010. Heterogeneity in astrocyte morphology and physiology. Brain Res. Rev. 63, 2–10. https://doi.org/10.1016/j.brainresrev.2009.12.001

Panickar, K.S., Norenberg, M.D., 2005. Astrocytes in cerebral ischemic injury: Morphological and general considerations. Glia 50, 287–298. https://doi.org/10.1002/glia.20181

Pannese, E., 2014. Neurocytology: fine structure of neurons, nerve processes, and neuroglial cells. Springer Berlin Heidelberg, New York, NY.

Pannese, E., Ferrannini, E., 1967. Nuclear pyknosis in neuroglia cells of normal mammals. Acta Neuropathol. (Berl.) 8, 309–319. https://doi.org/10.1007/BF00688831

Paternoster, M., Perrino, M., Travaglino, A., Raffone, A., Saccone, G., Zullo, F., D'Armiento, F.P., Buccelli, C., Niola, M., D'Armiento, M., 2019. Parameters for estimating the time of death at perinatal autopsy of stillborn fetuses: a systematic review. Int. J. Legal Med. 133, 483–489. https://doi.org/10.1007/s00414-019-01999-1

Pavelka, M., Roth, J., 2015. Functional ultrastructure: atlas of tissue biology and pathology. Springer Berlin Heidelberg, New York, NY.

Schäfer, A.Th., 2000. Colour measurements of pallor mortis. Int. J. Legal Med. 113, 81–83. https://doi.org/10.1007/PL00007713

Scheuerle, A., Pavenstaedt, I., Schlenk, R., Melzner, I., Rödel, G., Haferkamp, O., 1993. In situ autolysis of mouse brain: ultrastructure of mitochondria and the function of

oxidative phosphorylation and mitochondrial DNA. Virchows Arch. B Cell Pathol. Incl. Mol. Pathol. 63, 331–334. https://doi.org/10.1007/BF02899280
Sheleg, S.V., LoBello, J.R., Hixon, H., Coons, S.W., Lowry, D., 2008. Stability and Autolysis of Cortical Neurons in Post- Mortem Adult Rat Brains 9.
Stinnett, G.R., Lin, S., Korotcov, A.V., Korotcova, L., Morton, P.D., Ramachandra, S.D., Pham, A., Kumar, S., Agematsu, K., Zurakowski, D., Wang, P.C., Jonas, R.A., Ishibashi, N., 2017. Microstructural Alterations and Oligodendrocyte Dysmaturation in White Matter After Cardiopulmonary Bypass in a Juvenile Porcine Model. J. Am. Heart Assoc. 6. https://doi.org/10.1161/JAHA.117.005997
Suzuki, J., 2013. Treatment of cerebral infarction: experimental and clinical study., 1. ed. Springer, Tokyo.
Tomlinson, M., 2012. International Guidelines for the determination of death. Canadian Blood Services, Montreal.
Tsokos, M., Byard, R.W., 2016. Postmortem Changes: Overview, in: Encyclopedia of Forensic and Legal Medicine. Elsevier, pp. 10–31. https://doi.org/10.1016/B978-0-12-800034-2.00312-8
Xu, M., Zhang, H., 2011. Death and survival of neuronal and astrocytic cells in ischemic brain injury: a role of autophagy. Acta Pharmacol. Sin. 32, 1089–1099. https://doi.org/10.1038/aps.2011.50